1521-0103/385/1/35–49$35.00
THE JOURNAL OF PHARMACOLOGY AND EXPERIMENTAL THERAPEUTICS

dx.doi.org/10.1124/jpet.122.001384
J Pharmacol Exp Ther 385:35–49, April 2023

The Journal of PHARMACOLOGY And Experimental Therapeutics

Endothelial-Specific Targeting of RhoA Signaling via CD31 Antibody-Conjugated Nanoparticles[S]

Behnaz Lahooti, Racheal G. Akwii, Dhavalkumar Patel,[1] Siavash ShahbaziNia,[1] Margarita Lamprou, Mahboubeh Madadi, Thomas J. Abbruscato, Aristotelis Astrinidis, Ulrich Bickel, Abraham Al-Ahmad, Nadezhda A. German, George Mattheolabakis, and Constantinos M. Mikelis

Department of Pharmaceutical Sciences, School of Pharmacy, Texas Tech University Health Sciences Center, Amarillo, Texas (B.L., R.G.A., D.P., S.S., T.J.A., U.B., A.A.-A., N.A.G., C.M.M.); Laboratory of Molecular Pharmacology, Department of Pharmacy, University of Patras, Patras, Greece(M.L., C.M.M.); Department of Marketing and Business Analytics, Lucas College and Graduate School of Business, San Jose State University, San Jose, California (M.M.); Department of Pediatrics, University of Tennessee Health Sciences Center and Le Bonheur Children's Hospital, Memphis, Tennessee (A.A.); and School of Basic Pharmaceutical and Toxicological Sciences, College of Pharmacy, University of Louisiana Monroe, Monroe, Louisiana (G.M.)

Received July 25, 2022; accepted January 17, 2023

ABSTRACT

Existing vascular endothelial growth factor–oriented antiangiogenic approaches are known for their high potency. However, significant side effects associated with their use drive the need for novel antiangiogenic strategies. The small GTPase RhoA is an established regulator of actin cytoskeletal dynamics. Previous studies have highlighted the impact of endothelial RhoA pathway on angiogenesis. Rho-associate kinase (ROCK), a direct RhoA effector, is potently inhibited by Fasudil, a clinically relevant ROCK inhibitor. Here, we aimed to target the RhoA signaling in endothelial cells by generating Fasudil-encapsulated CD31-targeting liposomes as a potential antiangiogenic therapy. The liposomes presented desirable characteristics, preferential binding to CD31-expressing HEK293T cells and to endothelial cells, inhibited stress fiber formation and cytoskeletal-related morphometric parameters, and inhibited in vitro angiogenic functions. Overall, this work shows that the nanodelivery-mediated endothelial targeting of RhoA signaling can offer a promising strategy for angiogenesis inhibition in vascular-related diseases.

SIGNIFICANCE STATEMENT

Systemic administration of antiangiogenic therapeutics induces side effects to non-targeted tissues. This study, among others, has shown the impact of the RhoA signaling in the endothelial cells and their angiogenic functions. Here, to minimize potential toxicity, this study generated CD31-targeting liposomes with encapsulated Fasudil, a clinically relevant Rho kinase inhibitor, and successfully targeted endothelial cells. In this proof-of-principle study, the efficient Fasudil delivery, its impact on the endothelial signaling, morphometric alterations, and angiogenic functions verify the benefits of site-targeted antiangiogenic therapy.

Introduction

The effort to block angiogenesis in vascular-related diseases has been taking place for almost half a century with several promising angiogenesis inhibitors in the clinic (Pepper, 1997). However, several issues associated with their use as anticancer therapy prompt the interest in developing novel antiangiogenic approaches (Mattheolabakis and Mikelis, 2019). The bottleneck of antiangiogenic therapy is evasive resistance, the endothelial-derived resistance to angiogenesis inhibitors, via the upregulation and secretion of other growth factors, overcoming the blockade of vascular endothelial growth factor (VEGF) signaling, targeted by the majority of current antiangiogenic approaches (Wong et al., 2016; Zahra et al., 2021).

It is known that small GTPases regulate important biologic functions in endothelial cells, including mediation of angiogenesis (Tan et al., 2008; Barry et al., 2015; Nohata et al., 2016; Laviña et al., 2018). The initial role of the small GTPase Ras homolog family member A (RhoA) was determined in cell migration, where it is known to regulate the migratory potential of many cell types (Ridley, 2015). In endothelial cells, RhoA has been shown by our and others' work to regulate angiogenic and lymphangiogenic processes (Zeng et al., 2002; van Nieuw Amerongen et al., 2003; Mikelis et al., 2013; Zahra et al., 2019; Akwii et al., 2022). Most importantly, it is activated downstream of VEGF and regulates VEGF-driven endothelial functions (Zeng et al., 2002; van Nieuw Amerongen et al., 2003; Zahra et al., 2019). In

This work was supported for C.M.M. in part by the National Institutes of Health National Cancer Institute [Grant R15-CA231339], the Texas Tech University Health Sciences Center (TTUHSC) School of Pharmacy Office of the Sciences grant, and the Hellenic Foundation for Research and Innovation (00376), and for G.M. by the College of Pharmacy, University of Louisiana Monroe start-up funding, National Institutes of Health National Institute of General Medical Sciences [Grant P20-GM103424-21], and the Research Competitiveness Subprogram of the Louisiana Board of Regents through the Board of Regents Support Fund [LEQSF(2021-24)-RD-A-23]. The common TTUHSC equipment used was obtained through the Cancer Prevention Research Institute of Texas [Grants RP110786, RP190524, and RP200572]. The funders had no role in study design, decision to write, or preparation of the manuscript. The data were part of the Behnaz Lahooti's PhD Thesis at TTUHSC.
The authors declare no competing interests.
[1]D.P. and S.S. contributed equally to this work.
dx.doi.org/10.1124/jpet.122.001384.
[S] This article has supplemental material available at jpet.aspetjournals.org.

vivo, limited RhoA activation by combined global deficiency of PDZ-RhoGEF and leukemia-associated RhoGEF, two RhoA guanine nucleotide exchange factors and, thus, RhoA activators, led to embryonic lethality due to vascular deficiencies (Mikelis et al., 2013). Moreover, the downstream RhoA effector Rho-associated protein kinase (ROCK) is also considered pivotal for VEGF-induced angiogenesis regulation as ROCK inhibitors blocked VEGF-induced angiogenesis in vitro and in vivo (Bryan et al., 2010). However, the direct administration of ROCK inhibitors is expected, apart from suppressing the RhoA signaling in endothelial cells, to impact the RhoA-regulating functions of many cell types. To achieve higher endothelial specificity, we chose to explore delivering the ROCK inhibitor via targeted nanodelivery approaches.

The last few decades, liposomal formulations have been incorporated into clinical applications for cancer treatment, with Doxil leading the way of Food and Drug Administration approvals. Currently, several liposome-based formulations of active compounds are being evaluated in clinical trials (Bulbake et al., 2017). The liposomal hydrophobic bilayer surrounds a hydrophilic core, which allows the incorporation of both hydrophilic and hydrophobic compounds in their structure (Mattheolabakis et al., 2012b). The technological advances have led to the development of several variants of liposomal formulations depending on the need: i.e., long-circulating liposomes demonstrate prolonged presence in the circulation and rely on the incorporation of hydrophilic neutral polymers [predominately polyethylene glycol (PEG)] on the surface of the nanocarrier (Pattni et al., 2015).

To facilitate the need for tissue- and cell type–specific active targeting, the regular approach relies on the incorporation of a targeting moiety on the surface of liposomes, commonly attached to the distal end of the PEG molecules (Pattni et al., 2015). The active targeting moiety can be antibodies, antibody fragments, peptides, sugars, or others (Pattni et al., 2015; Zhang et al., 2020), and the principle relies on the overexpression of membrane receptors in certain cell types, especially under pathologic conditions (Akhtar et al., 2014). Active targeting moiety promotes the binding of the nanoparticles to membrane receptors, inducing the nanocarriers' accumulation on a specific cell type surface, which results in the local increase of the encapsulated drug and minimizes nonspecific accumulation in other tissues. Depending on whether the receptor can induce uptake, the drug can have an additional pathway to enter the targeted cell (Bazak et al., 2015; Attia et al., 2019).

In the present study, we aimed to specifically target the endothelial cells with the clinically relevant ROCK inhibitor Fasudil (F) (Nohria et al., 2006; Fava et al., 2012). We hypothesize that targeted delivery of Fasudil will block the RhoA signaling pathway in the endothelial cells and will inhibit their angiogenic potential. For this, we engineered liposomal nanoparticles decorated with cluster of differentiation 31 (CD31)-targeting antibodies, containing Fasudil, and evaluated their parameters, confirmed their selective binding to CD31-expressing cells, and explored the impact of the inhibition of the downstream RhoA molecular pathway in alteration of morphometric parameters, stress fiber formation, and in vitro angiogenic functions. Overall, this study provides a proof of principle for nanodelivery-based endothelial RhoA targeting, overcoming the side effects of nonspecific targeting of the RhoA pathway for more targeted therapeutic applications.

Materials and Methods

Materials. Lipids, 1,2-dipalmitoyl-sn-glycero-3-phosphocholine (DPPC) (Cat# 850355P), 1,2-dipalmitoyl-sn-glycero-3-phosphoethanolamine-N-[methoxy(polyethylene glycol)-2000] (ammonium salt) [(16:0 PEG2000 PE) Cat# 880160], and cholesterol from ovine wool (Cat# 700000P) were purchased from Avanti polar lipids, Inc. (Alabaster, Alabama). 1,2-Distearoyl-sn-glycero-3-phosphoethanolamine-N-[maleimide(polyethylene glycol)-2000] (ammonium salt) [(DSPE-PEG-Mal) 2000 molecular weight; Cat# PLS-9902] were purchased from Creative PegWorks (Chapel Hill, NC). Mouse Gamma Globulin Control (IgG), Invitrogen (Cat# 31878), and Mouse CD31 [platelet endothelial cell adhesion molecule 1 (PECAM-1)] rat anti-mouse antibody, Clone: 390, eBioscience (Cat# 50-125-22).

Cell Culture. The mouse brain endothelial cell line bEnd.3 (American Type Culture Collection, Cat# CRL-2299) used in this study was kindly provided from Dr. Abbruscato's laboratory at Texas Tech University Health Sciences Center, and the human embryonic kidney 293T (HEK293T; American Type Culture Collection, Cat# CRL-3216) cells were kindly provided by the Astrinidis laboratory at University of Tennessee Health Sciences Center. The cells were cultured in DMEM (Fisher Scientific, Cat# 11-995-073) supplemented with 10% FBS; Gibco; Cat# 10438026), 1X antibiotic-antimycotic solution (Gibco, Cat# 15240-062), and 1X nonessential amino acid (Gibco; Cat# 11-140-050). The cells were cultured on uncoated cell culture flasks as per manufacturer's protocols and maintained at 37°C with 5% CO_2 exposure. bEnd.3 cells were used between passages 24 and 29, and the medium was refreshed on every 3rd day (Prasad et al., 2017).

Human umbilical vein endothelial cells (HUVECs) were isolated from human umbilical cords obtained after C-sections. The protocol (A15-3891) was approved by the Texas Tech University Health Sciences Center Institutional Review Board, and informed consent was obtained from all donors. Cell culture of HUVECs took place in M199 medium (Corning, Cat# MT10060CV), with 15% FBS (Gibco; Cat# 10438026), 150 μg/ml endothelial cell growth supplement, 5 U/ml heparin sodium, and 1X antibiotic-antimycotic solution (Gibco, Cat# 15240-062), which was considered endothelial cell complete medium. Prior to HUVEC plating, the dishes were coated with 1% gelatin in PBS. Each HUVEC isolate was from a single donor, but the cells of at least two donors were used in the experiments to ensure reproducibility. HUVECs were used between passages 1 and 6. All cell cultures were maintained at 37°C and 5% CO_2 (Zahra et al., 2019).

Preparation and Purification of Nontargeting Liposomes. Fasudil liposomes (FLs) were prepared through thin-film evaporation technique. A mixture of lipids containing DPPC, cholesterol, and 16:0 PE-PEG 2000 PE, with the respective amount of 50, 11.2, and 6 mg, was used for the preparation of the liposomes. The lipids were dissolved in a 4:1 (V/V) mixture of chloroform and methanol (total volume, 10 ml). The total concentration of lipids in this preparation was 35 mM. The organic solvents were evaporated using a rotary evaporator (Buchi Rotor Evaporator R-210; BUCHI Labortechnik AG, Switzerland) at 45°C for ~3 hours to form a solid film in a round-

ABBREVIATIONS: Ab, antibody; CD31, cluster of differentiation 31; CD31FL, CD31-targeting Fasudil liposome; CD31L, CD31-targeting empty liposome; DLS, dynamic light scattering; DSPE-PEG-Mal, 1, 2-dostearoyl-sn-glycero-3-phosphoethanolamine-N-[maleimide (polyethylene glycol)-2000] (ammonium salt); F, Fasudil; FL, Fasudil liposome; HEK293T, human embryonic kidney 293T; HUVEC, human umbilical vein endothelial cell; IgGFL, IgG-conjugated Fasudil liposome; MLC, myosin light chain; MTT, 3-(4, 5-dimethylthiazol-2-yl)-2, 5-diphenyl-2H-tetrazolium bromide; PDI, polydispersity index; PECAM-1, platelet endothelial cell adhesion molecule 1; PEG, polyethylene glycol; pMLC, Phospho-Myosin Light Chain; RhoA, Ras homolog family member A; ROCK, Rho-associated protein kinase; RT, room temperature; TEM, transmission electron microscopy; VEGF, vascular endothelial growth factor.

bottom flask. Complete evaporation was achieved using a freeze dryer (LABCONCO, Cat# 7670520) for 30 minutes. The formed thin film was hydrated in either PBS to prepare nontargeted (empty) liposomes or a solution of Fasudil (LC Laboratories, Cat# F-4660) in PBS (25 mg/ml) to prepare Fasudil-encapsulated liposomes, followed by vigorous vortexing for 10 minutes to break the film (PBS, pH = 6.7, containing 0.1 M Na_2HPO_4 and 0.15M NaCl). The suspension was bath sonicated at 60°C for ∼1.5 hours. Then, probe sonication was performed (using Fisher Scientific; model, FB120 MODEL; power, 120W) at 60°C for ∼1 hour. The removal of nonencapsulated drug was achieved by passing the drug-loaded liposomes through a Sephadex-G-25 PD-10 column (Cytiva, Cat# 45-000-148) equilibrated with PBS (1X, pH 6.7) (Gupta et al., 2013).

Preparation and Purification of Antibody-Conjugated Liposomes. To prepare targeted liposomes, the postinsertion method was used to conjugate antibodies to the nanoparticles (Yang et al., 2018). For antibody conjugation, DSPE-PEG(2000)-Mal was added during liposome preparation. In parallel, an equal concentration (500 μg/ml) of antibodies (Ab) (mouse IgG and mouse CD31) was thiolated by mixing Traut's reagent (ThermoScientific, Cat# 26101) at a molar ratio of 1:5 and 1:10 of Ab:Traut's reagent, respectively. As per manufacturer's instructions, the mixture was incubated at room temperature (RT) under gentle continuous agitation for 1 hour in PBS containing 3.5 mM EDTA (pH 8.0). The nonreacted Traut's reagent was removed by Zeba spin desalting columns (ThermoScientific, Cat# 89891). The antibody (Ab) was conjugated to liposomes containing DSPE-PEG-Mal and incubated overnight at RT. The coupling reaction was performed under oxygen-free conditions using nitrogen atmosphere. As the maleimide group on DSPE-PEG-Mal is highly sensitive to the alkaline pH, to avoid rapid hydrolyzation of the maleimide group, the reaction was performed in PBS, pH 6.7.

2-Mercaptoethanol was used to cap the excess maleimide groups. Quenching of the reaction took place with 2 mM 2-mercaptoethanol for 30 minutes. The remaining nonreacted antibody was removed by ultracentrifugation at 60,000*g* at 4°C for 30 minutes and resuspension of liposomes in 800 μl PBS (1X, pH 6.7) thrice. After the purification, liposomes were stored at 4°C in the dark for a maximum 8-week period (Gholizadeh et al., 2018a). The conjugation of Ab to the liposomes was confirmed by gel electrophoresis.

Encapsulation Efficiency. A gradient ultraperformance liquid chromatography method was developed to quantify the amount of encapsulated Fasudil in liposomes. Fasudil content was detected at 320 nm, by disrupting the nanoparticles in (1%) Triton X-100 in PBS.

The analysis of Fasudil was performed using reverse-phase ACQUITY UPLC H-Class (Waters) with C8 column (Acquity, 50 mm × 2.1 mm, 1.7 μm) using the following parameter settings: the mobile phases (A) and (B) were 2 mM ammonium formate in water and ultraperformance liquid chromatography–grade methanol, respectively. The gradient elution was programmed as follows: 0 minutes 90% A; 0–2.00 minutes to 10% A; 2.00–3.00 minutes 10% A; 3.00–3.10 minutes to 90% A; and 3.10–4.00 minutes 90% A. The flow rate was set as 0.4 ml/min. The autosampler and column temperatures were 10°C and 40°C, respectively. The sample injection was performed using an automatic sampler, and the volume of injection was 2 μl. The following equation was used to calculate the drug encapsulation efficiency (Li et al., 2022):

$$\text{Drug encapsulation efficacy} = \text{Fasudil loaded in nanoparticles} / \text{total mass of Fasudil added initially} \quad (1)$$

Stability. Thirty microliters of nanoparticle suspension was mixed with 970 μl DMEM medium containing 10% FBS and incubated at 37°C in water bath. At specific time intervals, samples were withdrawn, and the particle size and ζ potential were measured by dynamic light scattering [(DLS) Malvern, Zetasizer, Nano-ZS90] (Lyu et al., 2019). For each sample, three measurements were taken with 10 runs per measurement. The particles' charge was measured for ζ potential, a reference parameter for colloidal stability. As a repellent surface force, this parameter contributes in the formulation stability by keeping the dispersed nanoparticles separate.

Storage Stability. The stability of the different liposomal nanoparticles was evaluated for 36 days. For this study, liposomes (500 μl) were stored at 4°C, and samples were withdrawn on days 0, 12, 24, and 36 and analyzed for particle size and polydispersity index (PDI), as described above.

Binding Studies. Liposome binding by b.End3 cells was determined by flow cytometry. One hundred thousand cells/well were cultured in a 12-well plate until 70% confluency was reached. Cells were incubated with liposomes in DMEM cell culture medium for 30 minutes, 1 hour, and 4 hours at 37°C. After removing the culture medium and excess of liposomes, the cells were washed three times with ice-cold PBS, trypsinized, and stained with secondary Alexa Fluor antibodies in the dark for 30 minutes. Binding of liposomes and secondary antibody by the cells was quantified via flow cytometry with BD FacsVerse. Generally, 10,000 events were acquired per sample (Gholizadeh et al., 2018a). The data were further analyzed by FlowJo and expressed as mean fluorescence intensity (Whittenton et al., 2013; Gholizadeh et al., 2018b).

Cell Transfection. The pcDNAI Neo mouse PECAM FL plasmid was a gift from Steven Albelda (Addgene plasmid # 42901; http://n2t.net/addgene:42901; RRID:Addgene_42901). The plasmid was transfected into HEK-293T cells using TurboFect Transfection Reagent (Thermo Fisher Scientific, Cat# R0533), PolyFect Transfection Reagent (Qiagen, Cat# 301105) and Lipofectamine 2000 (Thermo Fisher Scientific, Cat# 11668019) in antibiotic- and serum-free DMEM (with the exception of TurboFect, where we used complete media), following manufacturers' instructions. The media was changed to complete media after 6 hours. When the cells reached the ideal confluency the knocked-in efficiency was checked by flow cytometry, gel electrophoresis and western blot analysis before the cells were destined for further experiments (Sigurdardottir et al., 2021).

Phase Contrast Live Cell Imaging. Twenty thousand b.End3 cells/well were cultured on 24-well glass plates (24-well glass-bottom plates, Cellvis Cat#P24-1.5H-N) overnight. The next day, cells were rinsed twice with PBS to remove any dead cells and debris and replaced with fresh complete medium. The plate was then carefully mounted onto the Livecyte (by Phasefocus), machine and constant acquisition was commenced at determined time points for 24 hours.

Cell Viability Assay. The 3-[4, 5-dimethylthiazol-2-yl]-2, 5- dimethyltetrazolium bromide [(MTT) Fisher; Cat# AC15899] colorimetric assay was used to evaluate cell viability (Zahra et al., 2019). Eight thousand cells in 200 μl of complete media were seeded in each well of a 96-well plate and incubated for 48 hours at 37°C under 5% CO_2.

After that period, the cells were treated with Fasudil or Fasudil-encapsulated liposomal nanoparticles for 48 hours. At the end of the incubation period, 20 μl of MTT stock solution (5 mg/ml in PBS) was added in each well for 2 hours to allow formazan crystal formation. Then, the medium was removed, and formazan crystals were dissolved with 100 μl DMSO upon agitation for 10 minutes. The absorbance values were obtained using a microplate reader at 570 nm (Twentyman and Luscombe, 1987).

Immunoblotting. Protein expression and activation analysis was performed as previously reported (Zahra et al., 2019; Akwii et al., 2022). Briefly, the cells were lysed on ice in RIPA buffer (10 mM Tris-HCl, 1 mM EDTA, 0.5 mM EGTA, 1% Triton X-100, 0.1% sodium deoxycholate, 0.1% SDS, and 140 mM NaCl) in the presence of protease and phosphatase inhibitors (Halt Protease and Phosphatase Inhibitor Cocktail, Thermo Scientific, Cat# 78445) unless specified. The cell lysates were centrifuged at 12,000*g* for 5 minutes at 4°C. Upon elution of the supernatant in Laemmli sample buffer, the samples were heated at 95–100°C and centrifuged briefly at maximum speed. Equal amounts of proteins were subjected to SDS-PAGE electrophoresis and transferred on a polyvinylidene difluoride membrane (Immobilon P, Millipore Sigma, Cat# IPVH304F0).

The membranes were blocked with 5% milk in Tris-buffered saline/Tween 20 and probed with primary antibodies for Phospho-Myosin Light Chain [(pMLC) 1:1,000; Cell Signaling Technology, Cat#3674],

Tubulin (1:2000; Cell Signaling Technology, Cat#2146), CD31 (PECAM-1; 89C2; 1:1,000; Cell Signaling Technology, Cat#3528), and secondary anti-rabbit (Southern Biotech, Cat# 4010-05) and anti-mouse (Southern Biotech, Cat# 1010-05) horseradish peroxidase–conjugated antibodies. Immunoreactive bands were visualized by Immobilon Western Chemiluminescent HRP Substrate (Millipore Sigma, Cat# WBKLS0500), and the quantification of intensity of the immunoreactive bands took place with the ImageJ image analysis software (National Institutes of Health).

Immunofluorescence Staining and Confocal Microscopy. For the immunofluorescence experiments, the cells were seeded on circular cover glasses (Fisherbrand, Cat# 12-545-80) in a 24-well plate. At about 70% confluency, the cells were treated with F, Fasudil liposomes (FL), CD31-targeting Fasudil liposomes (CD31FL), CD31-targeting empty liposomes (CD31L), and IgG-conjugated Fasudil liposomes (IgGFL) for 30 minutes, 1 hour, and 4 hours. The cells were treated with 30 μM of Fasudil (free or encapsulated) in all treatment groups, and the concentration of the liposomes was adjusted to refer to the same Fasudil concentration. After treating all groups at 37°C, the cells were fixed with 4% paraformaldehyde in PBS for 10 minutes at RT. Then, they were stained with Alexa Fluor 488 Phalloidin (Molecular Probes, Cat# A12379) for 45 minutes at RT and washed three times with PBS. Cell nuclei were stained with Hoechst (1:2000 in PBS; Molecular Probes, Cat# 33342). After mounting, the slides were left in the dark at RT for 2 hours before storage at 4°C. Stained samples were imaged using a Leica TCS SP8 confocal microscope. All laser parameters were maintained throughout all experimental samples. For each experiment, 5–10 images at the same focal plane were taken for further evaluation (Girão-Silva et al., 2021).

Tube Formation Assay. Matrigel tube formation assay was performed as previously described (Mikelis et al., 2011). Briefly, 40 μl of reduced growth factor–Basement Membrane Extract (Trevigen, Cat# 3433) were added in each well of a 96-well plate. The extract was left to polymerize for 20 minutes at 37°C with 5% CO_2. b.End3 cells were resuspended in either starvation medium or complete medium and quantified. Fifty thousand or 70,000 cells per well were added in starvation or full medium, as indicated, and were incubated for 6 hours at 37°C with 5% CO_2. After optimization of the experimental conditions (fewer than 50,000 b/End3 cells/well did not provide sprouts in our experimental settings), 70,000 cells/well in the different groups were treated with F, FL, CD31FL, CD31L, and IgGFL. The concentration of Fasudil for all groups was 30 μM. Sprout images were obtained by a bright-field microscope (Microscoptics, IV-900) connected with a digital camera (AmScope FMA050) in the 4× magnification. The quantification of number of nodes, number of junctions, and total sprout length was achieved with the "Angiogenesis Analyzer" plug-in in ImageJ image analysis software (National Institutes of Health).

Cell Migration Assay. The cell migration experiments were performed in 48-well Boyden chambers with 8-μm pore polyvinyl pyrrolidone-free polycarbonate membranes (NeuroProbe, Cat# PFB8) as previously reported (Mikelis et al., 2013). The membranes were precoated with collagen (10 μg/ml). After a 4-hour starvation, the b.End3 cells were trypsinized and centrifuged. Pretreated cells with F, FL, CD31FL, CD31L, and IgGFL for 4 hours at 37°C were added to the upper chamber, and DMEM without FBS was added to the lower chamber. In both lower and upper chambers, the concentration of free or liposome-encapsulated Fasudil corresponded to 30 μM. Upon pretreatment, 50,000 cells were resuspended in 50 μl starvation medium in the presence of treatment and added in the upper compartment of each well, with the same treatment happening in the lower compartment. The cells were incubated for 6 hours at 37°C with 5% CO_2. At the end of the incubation period, the membrane was fixed (methanol for 10 minutes at RT), stained for hematoxylin (40 minutes at RT), washed twice (dH_2O), and stretched on a glass slide with the lower side facing down. All cells on the top (nonmigrating) were carefully removed, and migrating cells (lower side) were counted at a brightfield microscope (Microscoptics, IV-900) at 40X magnification. The quantification took place in a blinded manner.

Cryo Sample Preparation for Transmission Electron Microscopy Analysis. Three microliters of sample solution was applied to a 300-mesh Lacey Carbon film grid (EMS LC300-CU-150). The blotting procedure and the quenching of specimens were performed with a cryoplunge 3 (gatan) using 1.7-second plotting time. After cold stage transfer, the samples were mounted and examined in JEOL JEM 1400 electron cryo-microscope (Japan) operating at an accelerating voltage of 120 kV. The stage temperature was kept below −170°F, and images were recorded at defocus setting with gatan US1000xp2 camera.

Statistical Analysis. All experiments were repeated at least three times with similar results. For two independent groups, statistical analysis was performed by unpaired two-tailed Student's t test, and for more than two independent groups, statistical analysis was performed by one-way ANOVA, followed by Dunnett's multiple comparisons test. GraphPad Prism version 9.00 for Windows (GraphPad Software, San Diego, CA) was used for data analysis, and the results were expressed as mean ± S.E.M. The asterisks in the figures denote statistical significance (*$P < 0.05$; **$P < 0.01$; ***$P < 0.001$).

Results

Preparation and Characterization of Immunoliposomes

The liposomes in this study were prepared using the thin-film evaporation technique. The lipids were dissolved in chloroform and methanol, and upon evaporation of the organic solvents, the film was hydrated in PBS in the presence or absence of Fasudil. The strategy for the preparation of the liposomes (FL as nontargeted particles, CD31FL as treatment liposomes, and IgGFL as antibody-carrying negative control liposomes), as described in detail in *Materials and Methods*, is illustrated in Fig. 1. The CD31 antibody and IgG antibody were covalently linked to DSPE-PEG-Mal by Traut's reagent via maleimide-thiol coupling reaction.

The physicochemical properties of all Fasudil-loaded liposomes were within acceptable range (Fig. 2A). The average liposomal sizes, determined by DLS, of CD31FL and IgGFL were 170.0 ± 6.7 nm and 173.2 ± 6.7 nm, respectively, with no statistically significant difference, compared with FL, of which the particle size was 158.0 ± 12.7 nm, suggesting that the coupling process did not significantly impact the vehicle size. The prepared liposomes showed a slightly negative ζ potential of around −17 mV (Fig. 2A), which is expected due to the localized negative charges on the phospholipid head groups in the liposomal bilayer. The PDI was in the range of 0.15 and 0.20 (Fig. 2A), suggesting that the formulations had a relatively narrow size distribution. The above physicochemical properties were in agreement with other studies (Lu et al., 2018; Lyu et al., 2019; Sun et al., 2019; Wang et al., 2021). The average Fasudil encapsulation efficiency was around 3%–6%, resulting in an average loading content of approximately 0.350 mg/ml (antibody-conjugated liposomes) to 0.7 mg/ml (nontargeted Fasudil liposomes) for different particles (Fig. 2A). Similar encapsulation efficiencies have been reported for the film hydration method of hydrophilic drugs (Gholizadeh et al., 2018a). Transmission electron microscopy (TEM) images verified that the liposomal nanoparticles had a round, well defined spherical shape with a smooth surface (Fig. 2B). The formulations showed little to no aggregations, indicating that the nanoparticles were homogeneously dispersed, which was in line with the DLS results (Fig. 2A).

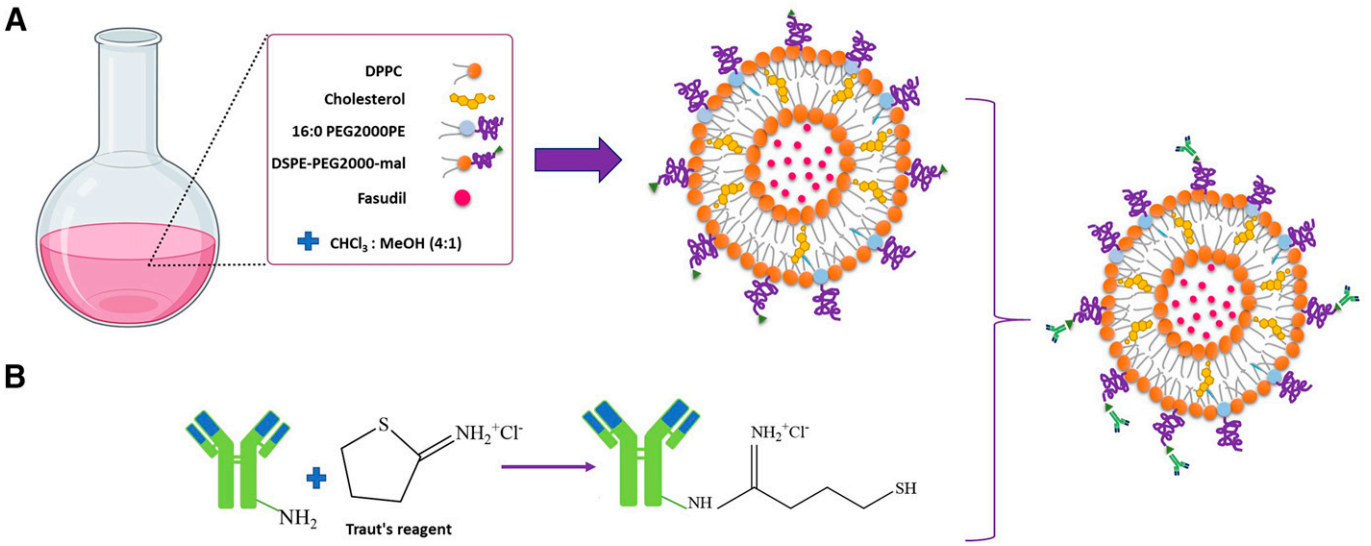

Fig. 1. Preparation strategy of Ab-conjugated liposomes. Schematic representation of (A) liposome formation and (B) antibody conjugation strategy. Antibody-liposomal conjugation took place via reaction with Traut's reagent.

Storage Retention and Stability of the Immunoliposomes

One of the greatest challenges in nanoparticle design is to increase their potency to sufficiently reach the therapeutic site while minimizing undesired accumulation (Barua and Mitragotri, 2014). As the stability of nanoparticles in serum is indicative for their targeting potential, their stability was studied

A

Formulation	Size (nm)	ζ potential (mV)	PDI	EE%
FL	158.0 ± 12.7	−16.10 ± 0.90	0.147 ± 0.002	6.70 ± 0.2
IgGFL	173.2 ± 6.7	−17.00 ± 1.05	0.206 ± 0.002	4.10 ± 0.16
CD31FL	170.0 ± 6.7	−17.20 ± 0.97	0.166 ± 0.005	3.90 ± 0.30

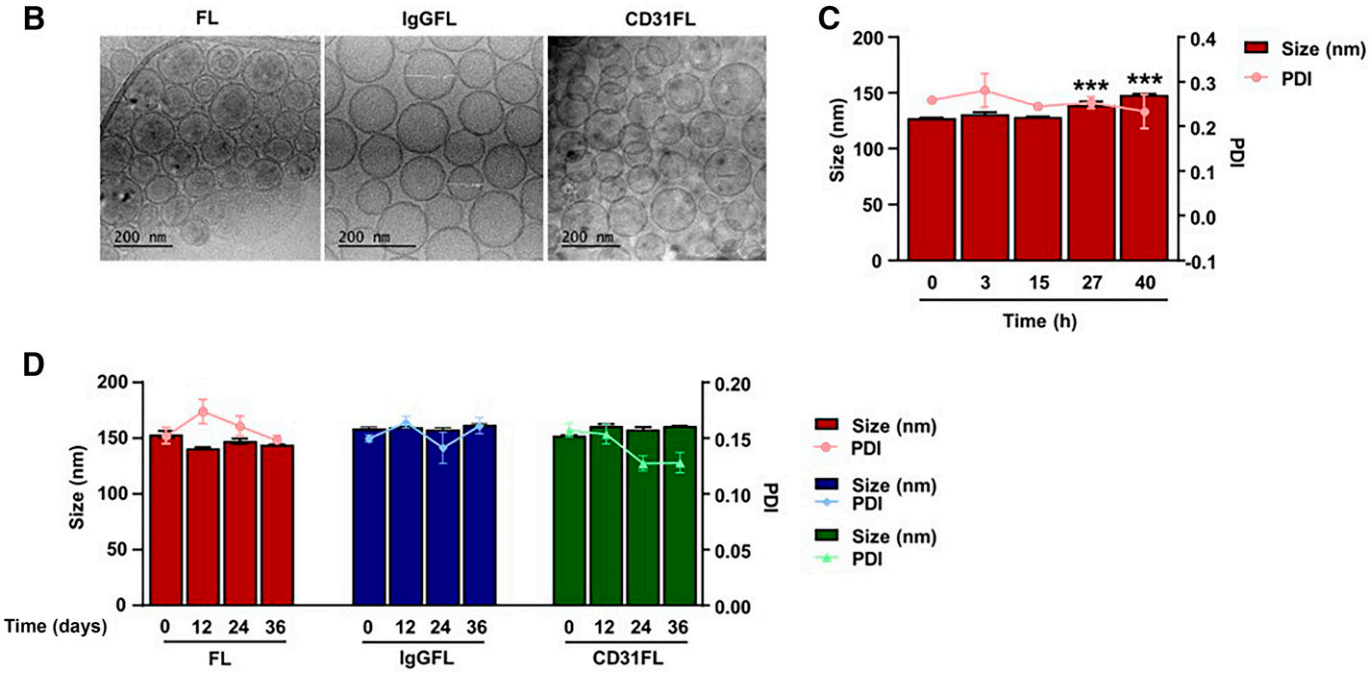

Fig. 2. Liposomal characterization. (A) Table summarizing the average size, ζ potential, PDI, and percentage of encapsulation efficiency (EE). (B) TEM images of FL, IgGFL, and CD31FL. Scale bar, 200 nm. (C) Stability assessment of FL in terms of size and PDI for 40 hours in media containing 10% FBS at 37°C (size in all time points compared with that of time 0) (n = 3). (D) Assessment of storage stability of 4°C based on size and PDI of the FL, IgGFL, and CD31FL liposomes (size in all time points compared with that of time 0 for each liposomal group) (n = 3).

by measuring the changes in particle size and PDI using the DLS method. The liposomal formulations were dispersed in 10% FBS medium for 40 hours at 37°C, and the particle size was measured at predetermined time points. The particle size and PDI of FL were not altered within the first 15 hours (Fig. 2C), indicating that FL presented high stability within at least the first 15 hours at 37°C. After that point, the stability of the particles was lightly affected, demonstrating an expected (Lyu et al., 2019) slight increase in the size of the particles and their respective PDI values.

To further examine the stability of the formed liposomes, we assessed potential alterations in particle size and PDI of formulations under storage. The particle size and PDI of the formulations were monitored for almost 5 weeks when stored at 4°C. We observed no changes in size and PDI in the formulations stored at 4°C, suggesting that the vesicles remained separated, and no appreciable aggregation during the storage period took place (Fig. 2D). It should be noted that the values in Fig. 2, C and D are generated by the average size of each batch measured and not by the extreme values of individual liposomes per batch.

Evaluation of Antibody Conjugation on the Liposomal Nanoparticle Surface

We next sought to confirm whether the murine CD31 and IgG antibodies had been covalently coupled to the liposomal surface. The coupling, mediated by Traut's reagent, occurred via the addition of a thiol group to the antibody and the reaction with the DSPE-PEG-Mal (Hermanson, 2013; Ravasco et al., 2019). Next, immunoblotting was performed to check for the presence of antibodies on the liposomal nanoparticles (Fig. 3A). Free murine CD31 and IgG antibodies were added as control and migrated as two bands of approximately 25 and 55 kDa, which correspond to the light and heavy chains of the antibody, respectively (Fig. 3A). Control (nontargeted) FLs showed no bands, whereas CD31FL and IgGFL showed bands at 25 and 55 kDa, corresponding to the molecular mass of antibody heavy or light chains coupled to the liposomes (Fig. 3A).

The unconjugated antibodies were separated from the ones conjugated to the liposomal nanoparticles through ultracentrifugation, and the purity of the particles or removal of free antibodies was assessed by immunoblotting (Fig. 3, B and C). For this, the antibody presence was monitored in particles and supernatant after every 30 minutes of purification and replacement with fresh PBS. As observed, both particles and supernatant after 30 minutes of centrifugation at 60,000*g* showed two bands of approximately 25 and 55 kDa, which correspond to the light and heavy chains of the antibodies, respectively. However, after removal of the supernatant, resuspension of the liposomes, and additional 30-minute centrifugation (two times), i.e., 1-hour and 1.5-hour time points, only the CD31FL and IgGFL particles showed the corresponding antibody bands, but no antibody was detected in the supernatant. These results demonstrated that upon use, the liposomal nanoparticle solution did not contain free antibodies, which was important for the proper binding estimation.

Evaluation of Binding Specificity of the Immunoliposomes

Since our liposomes were designed to target the CD31-expressing endothelial cells, we first wanted to evaluate their binding specificity. Thus, we generated an artificial expression system by transfecting HEK293T cells, which lack CD31 expression, with a plasmid encoding murine CD31. We evaluated several transfection reagents for their transfection efficiency (Fig. 4, A and B) and selected Lipofectamine 2000 for further studies. To evaluate the binding of the CD31FL particles on the murine CD31-expressing or control HEK293T cells, we detected the CD31 antibody presence by the specific binding of the specific fluorescein isothiocyanate–conjugated secondary antibody (Whittenton et al., 2013). The selective binding of the CD31FL liposomes upon CD31 expression was verified at all evaluated time points (0.5 hours, 1 hour, 4 hours; Fig. 4C). In all time points, the comparative binding of the control liposomal nanoparticles (FL, IgGFL) with the CD31FL verified the specific binding of the CD31FL on CD31-expressing cells (Fig. 4D).

We then evaluated murine CD31 expression in various murine and human cell lines, such as the human primary endothelial cells (HUVECs; Fig. 4A), the murine macrophage cell lines Raw264.7 and J774.1, and the murine brain endothelial cell line b.End3 (Fig. 5A). CD31 expression was assessed by immunoblotting (Figs. 4A and 5A) and flow cytometry (not shown). As expected, the b.End3 cells presented strong CD31 expression and were subsequently selected for the study. Similar to the CD31-expressing HEK293T cells, the binding of the CD31FL on the b.End3 cells was specific and significant in all three time points assessed (Fig. 5, B and C). Our findings are in agreement with previous results of the secondary antibody-based immunoliposome detection method (Lu et al., 2018)

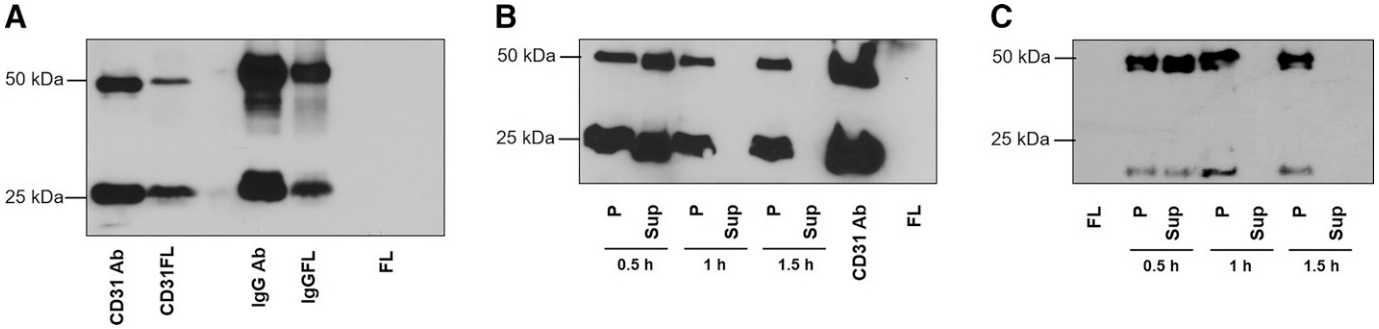

Fig. 3. Evaluation of conjugation of antibodies to the surface of the liposomal nanoparticles. (A) Representative western blot image demonstrating IgG and CD31 antibody conjugation on the liposomes. Pure isolated antibody was run as positive control. (B and C) Representative western blot images demonstrating the liposomal nanoparticle purification after antibody conjugation of (B) CD31 and (C) IgG antibodies. Liposome particle (P) versus the supernatant of the same sample (Sup) after 0.5, 1 (2 × 30 minutes), and 1.5 hours (3 × 30 minutes) of centrifugations. Commercial CD31 antibody was run as positive and Fasudil liposomes were run as negative controls.

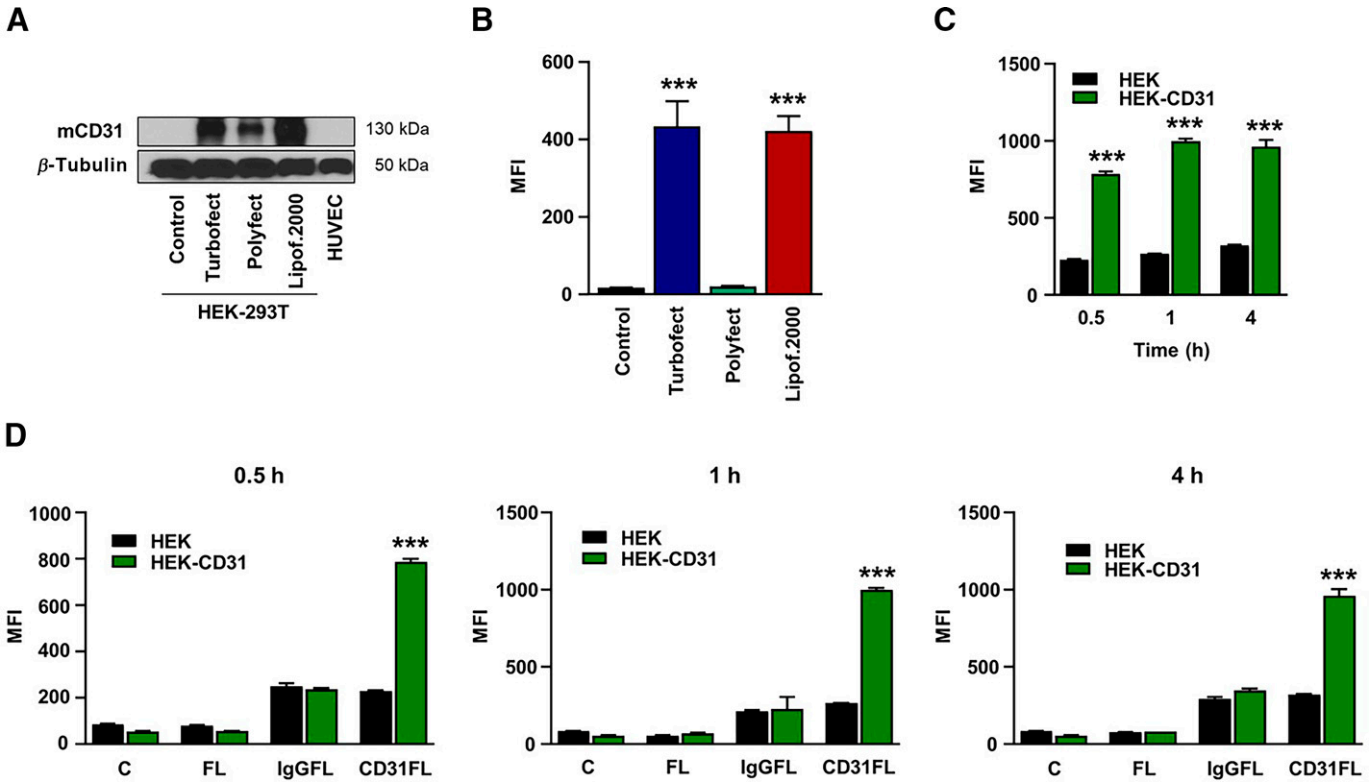

Fig. 4. Assessment of binding of CD31-targeting liposomal nanoparticles on CD31-expressing HEK293T cells. (A) Representative western blot images and (B) flow cytometry quantification of HEK293T cells without or with murine CD31 expression upon transfection with different transfection reagents. Transfection with lipofectamine 2000 (Lipof.2000) was further used for the binding experiments (groups compared with the mock-transfected control group) ($n = 3$). (C) Flow cytometry graphs representing binding of CD31 antibody-conjugated Fasudil liposomes (CD31FL) in HEK293T cells expressing or not expressing murine CD31 at 37°C under 0.5, 1, and 4 hours of incubation (binding on CD31-expressing cells compared with binding of non–CD31-expressing cells for each time point) ($n = 3$). (D) Flow cytometry graphs representing comparative binding of FL, IgGFL, and CD31FL in each respective time point of incubation (each CD31-expressing group compared with the nonexpressing group of the specific treatment and time point) ($n = 3$). ***$P < 0.001$. C, control; CD31FL, CD31-targeting Fasudil liposomes; FL, Fasudil liposomes; IgGFL, IgG-conjugated Fasudil liposomes; MFI, mean fluorescence intensity.

since CD31FL showed stronger binding compared with the other particles, confirming the CD31-dependent mechanism.

Toxicity Studies of Fasudil and Fasudil-Encapsulated Liposomes on b.End3 Cells

To investigate the in vitro cytotoxicity of the liposomes, an MTT assay was performed on the b.End3 cells following treatment with Fasudil, FL, or CD31FL. Free Fasudil was initially tested over a wide range of concentrations (up to ~5 mM) and showed an IC_{50} value of 90.21 ± 4.66 μM (Fig. 6, A and E). Based on this IC_{50}, the Fasudil-containing liposomes were tested within a concentration range of 0–320 μM and showed an IC_{50} of 187.5 ± 8.21 μM (Fig. 6, B and E), higher than the free drug (Fig. 6, A and E), and the IgGFL presented a similar trend (Fig. 6, D and E). CD31FL treatment increased the cells' survival rate, with an IC_{50} of 211.6 ± 14.00 μM (Fig. 6, C and E). Conjugation of the CD31-targeting antibody did not substantially alter the CD31FL IC_{50} from the FL one, and the IC_{50} was still higher than free Fasudil (Fig. 6E). This could be explained as Fasudil's target, ROCK, is a known regulator of both early and late apoptotic stages (Shi and Wei, 2007); thus, increased Fasudil incorporation in nontoxic concentrations could potentially increase survival. Another explanation could be limited uptake due to steric hindrance (Botosoa et al., 2011; Ringgaard et al., 2020), which would still provide advantage for potential in vivo applications. Free CD31-targeting antibodies are normally not internalized per se in endothelial cells, but when conjugated to nanocarriers, they are internalized via a noncanonical endocytic pathway (Han et al., 2012), and as noninternalizable endothelial antigens, they support stable and prolonged endothelial targeting. CD31-targeting nanoparticles have shown endothelial-specific targeting, especially in the lungs (Parhiz et al., 2018). However, the endocytosis of the nanoparticles depends on the flow and the CD31 epitopes targeted (Han et al., 2012, 2015). RhoA activation and stress fiber formation inhibits CD31-mediated internalization (Han et al., 2012), whereas on the other hand, RhoA activation is important for endocytosis of CD31-targeting nanoparticles (Garnacho et al., 2008), upon which we aim to block the pathway in the endothelial cells. The advantage of CD31 targeting is the preservation of endothelial barrier function (Garnacho et al., 2008) and, thus, the reason it was selected for our study. It is considered that noninternalizable endothelial antigens support stable and prolonged endothelial targeting (Murciano et al., 2001), which supports the use of CD31-targeting nanoparticles for endothelial RhoA inhibition.

Fasudil and Fasudil-Encapsulated Liposomes Inhibit Myosin Light Chain Phosphorylation in b.End3 Cells

Fasudil is a clinically relevant inhibitor of ROCK, the direct RhoA downstream target (Nohria et al., 2006; Fava et al., 2012). Downstream of ROCK is the myosin light chain (MLC), which is involved in the rearrangement of actin cytoskeleton (Matsui et al., 1996; Mikelis et al., 2015). To assess the lowest Fasudil

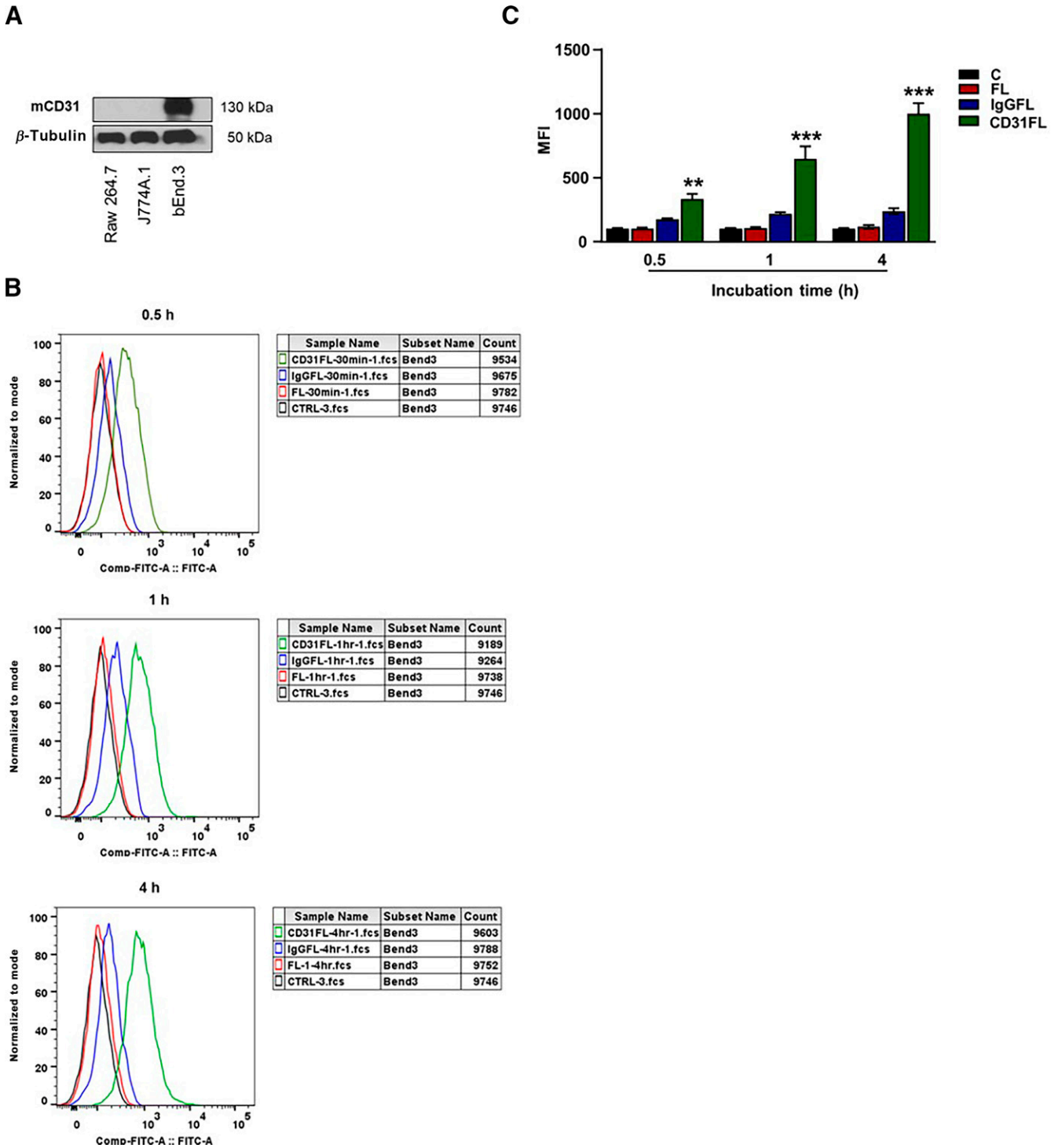

Fig. 5. Assessment of liposomal nanoparticles' binding on b.End3 cells. (A) Representative western blot images of murine CD31 expression on b.End3 cells. (B) Flow cytometry graphs representing the binding of FL, IgGFL, and CD31FL at 37°C for 0.5, 1, and 4 hours. (C) Quantification of the liposome binding by secondary antibody (each group compared with the control group of the specific time point) ($n = 3$). $^{**}P < 0.01$; $^{***}P < 0.001$. C, control; CD31-targeting Fasudil liposomes; Comb-FITC-A, combination of FITC-A expression of all samples; FITC-A, fluorescein isothiocyanate-A; FL, Fasudil liposomes; IgGFL, IgG-conjugated Fasudil liposomes; MFI, mean fluorescence intensity.

concentration offering a significant inhibition of MLC phosphorylation in b.End3 cells, dose-dependent western blot experiments were performed following Fasudil treatment to quantify the levels of pMLC using thrombin as an activator of the ROCK/pMLC pathway (Mikelis et al., 2013) (Fig. 7, A and B). Following a 4-hour FBS starvation period, Fasudil treatment of 30 minutes inhibited basal and thrombin-induced MLC phosphorylation at tested concentrations of 10–40 μM, with the 30-μM concentration showing a more consistent effect (Fig. 7, A and B). Based on the fact that the 30 μM of Fasudil has no effect on cell viability

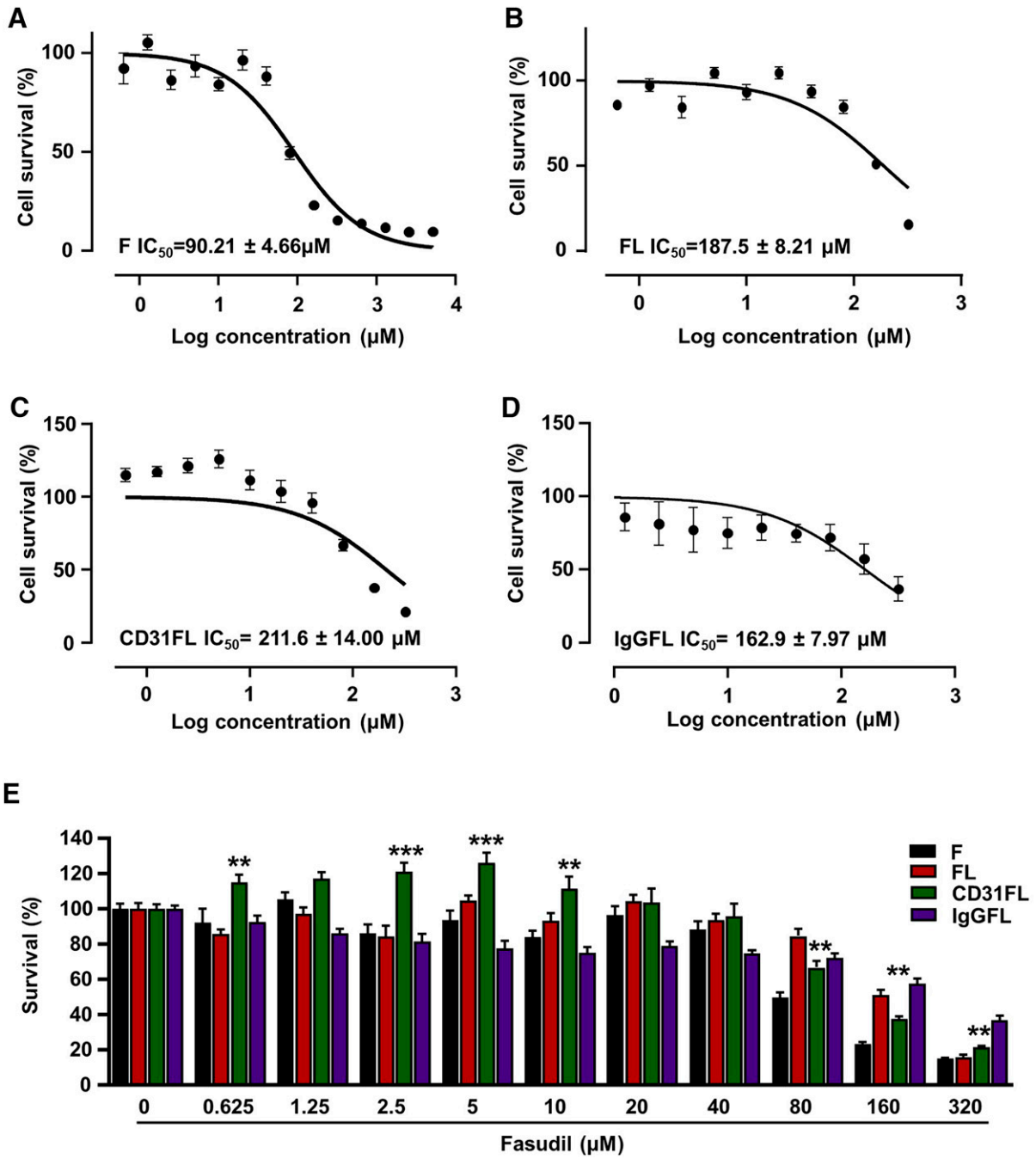

Fig. 6. Free and Fasudil-encapsulated liposome IC_{50} evaluations on b.End3 cells. The IC_{50} evaluation of (A) Fasudil (Fas), (B) FL, (C) CD31FL, and (D) IgGFL in b.End3 cells. (E) Comparative assessment of b.End3 cell survival on different concentrations of free Fasudil treatment and Fasudil-encapsulated liposomes. Comparison of CD31FL with F treatment of each concentration ($n = 3$). $^{**}P < 0.01$; $^{***}P < 0.001$. CD31FL, CD31-targeting Fasudil liposomes; F, Fasudil; FL, Fasudil liposomes; IgGFL, IgG-conjugated Fasudil liposomes.

(Fig. 6) while showing consistent inhibition of the downstream pathway (Fig. 7, A and B), we selected this dose for liposome encapsulation for our downstream applications.

Next, we evaluated the levels of MLC phosphorylation in the presence or absence of thrombin upon treatment of F, FL, IgGFL, and CD31FL. All liposomal formulations showed higher potency to inhibit MLC phosphorylation compared with free Fasudil (Fig. 7, C and D), with CD31FL having the more pronounced effect, potentially due to the CD31 targeting. To evaluate the specificity of the CD31FL on endothelial cells, we repeated the same experiments with CD31FL and IgGFL treatment in non–CD31-expressing cells (HEK293T), with comparable inhibitory effect between IgGFL and CD31FL treatments, profoundly due to similar nonspecific binding (Supplemental Fig. 1).

Effect of Fasudil and Liposome Treatment on the Morphometric Properties of the Cells

Given that RhoA signaling regulates the actin cytoskeleton dynamics, we first wanted to explore whether incorporation of the Fasudil-containing liposomes affects morphometric parameters of the b.End3 cells. Thus, we performed morphometric

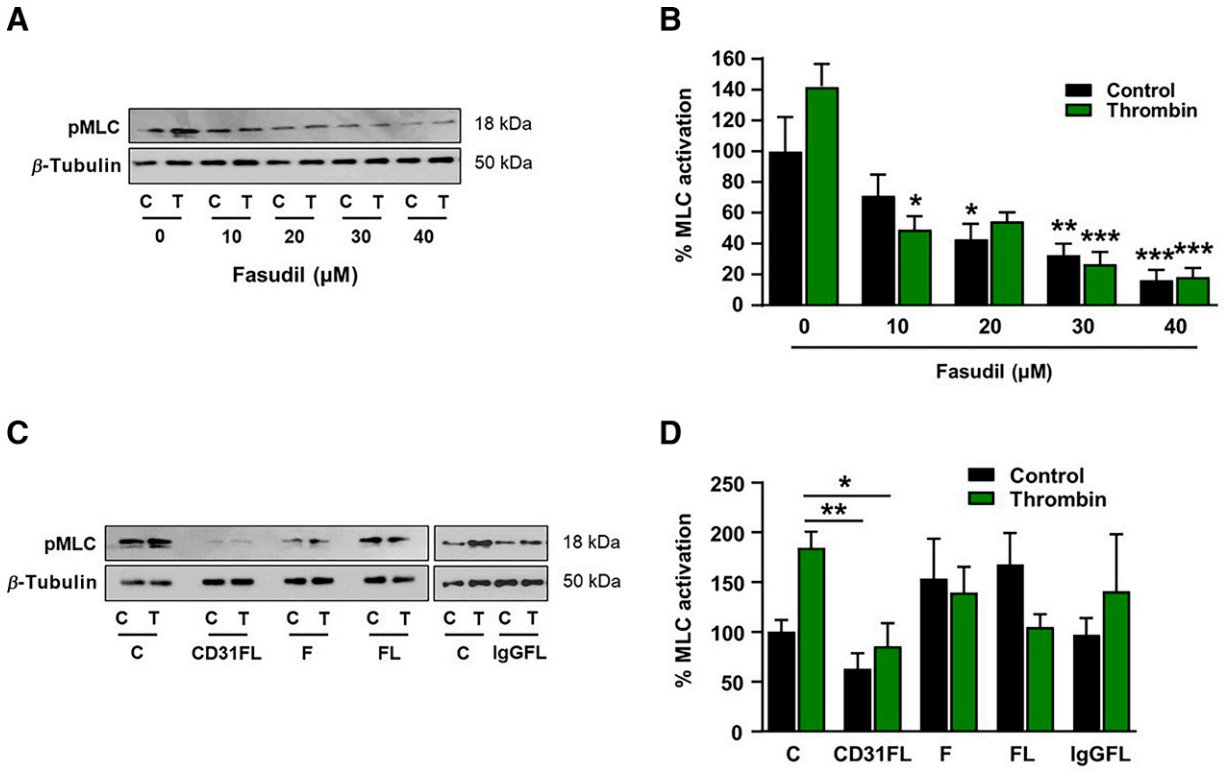

Fig. 7. Fasudil dose-response effect on MLC activation in b.End3 cells. (A) Representative western blot images and (B) quantification of MLC activation on b.End3 cells after treatment with different with thrombin and different Fasudil concentrations for 30 minutes upon 4-hour starvation (groups compared with nontreated cells) ($n = 4$). (C) Representative western blot images and (D) quantification of MLC activation on b.End3 cells after treatment of FL, IgGFL, CD31FL, and IgGFL upon 4-hour starvation (groups compared with thrombin-induced pMLC of untreated cells) ($n = 3$). *$P < 0.05$; **$P < 0.01$; ***$P < 0.001$. C, control; CD31FL, CD31-targeting Fasudil liposomes; F, Fasudil; FL, Fasudil liposomes; IgGFL, IgG-conjugated Fasudil liposomes.

analysis of the cells treated with F, FL, CD31FL, or IgGFL. To ensure that the effect is strictly Fasudil related and to exclude potential CD31 Ab-mediated effects on cellular morphometric alterations, we included as additional control, CD31 Ab-conjugated blank liposomes (CD31L). Morphometric analysis was performed via phase contrast–based live cell imaging, and different cell structural properties were analyzed. Biologically relevant parameters can be directly interpreted from the phase profile of the cells due to their heterogeneous refractive index (Girshovitz and Shaked, 2012). We had previously shown that RhoA activation induces cell retraction, thus inducing cell sphericity (Mikelis et al., 2013; Zahra et al., 2019). b.End3 cell sphericity was decreased upon FL, CD31FL, and IgGFL treatment, whereas no effect was observed in the control, Fasudil, or CD31L groups (Fig. 8A). At the steady-state conditions, Fasudil acts uniformly over the cellular area, preserving the shape and inhibiting actin rearrangement functions. Liposomal incorporation is expected to alter the cellular shape, but this alteration seems to be absorbed by adjustment of the actin cytoskeleton (CD31L), which is blocked when Fasudil is present (FL, IgGFL, CD31FL). In a similar manner upon cell retraction, the cellular perimeter decreases. The perimeter of the Fasudil-, FL-, CD31FL-, and IgGFL-treated cells increased, contrary to the perimeter of the CD31L-treated cells, which was closer to the control levels (Fig. 8B). The area of FL-, CD31FL-, and IgGFL-treated cells also increased significantly, with a smaller, but statistically significant, increase in the Fasudil group and no increase in the CD31L group, demonstrating that this change is due to Fasudil effect and is not related to liposomal- or CD31-induced effects (Fig. 8C). The decrease in sphericity can be attributed to the blockade of RhoA signaling, which is concomitant with the increase in the area and perimeter. The controlled Fasudil release has more impact on morphometric parameters than the free drug, confirming efficient inhibition of the endothelial (b.End3) RhoA signaling upon treatment with Fasudil-containing liposomes.

Antibody-Conjugated Fasudil Liposomes Inhibit Stress Fiber Formation in b.End3 Cells

Since the ROCK/pMLC pathway is involved in the rearrangement of actin cytoskeleton (Matsui et al., 1996; Mikelis et al., 2015), we further explored the effect of the conjugated liposomes on stress fiber formation. Cellular actin was stained with fluorescent phalloidin upon Fasudil or liposome treatment of a time range of 30 minutes, 1 hour, and 4 hours. FL, IgGFL and CD31FL treatment inhibited stress fiber formation as early as 30 minutes, and this effect was sustained up to 4 hours, with CD31FL having the most prominent effect (Fig. 8D). Contrary to the Fasudil-encapsulated liposomes, the CD31L had no observable effect on the stress fiber formation (Fig. 8D). This demonstrates that liposome-encapsulated Fasudil is responsible for the inhibitory effect of stress fiber formation, the efficiency of which was augmented upon CD31 conjugation with the Fasudil-containing liposomes.

Antibody Conjugation of Fasudil Liposomes Induces Its Inhibitory Effect on in Vitro Angiogenesis in b.End3 Cells

The ROCK inhibitor Fasudil inhibits in vitro and in vivo angiogenesis in both endothelial cells and cancer cells (Yin et al.,

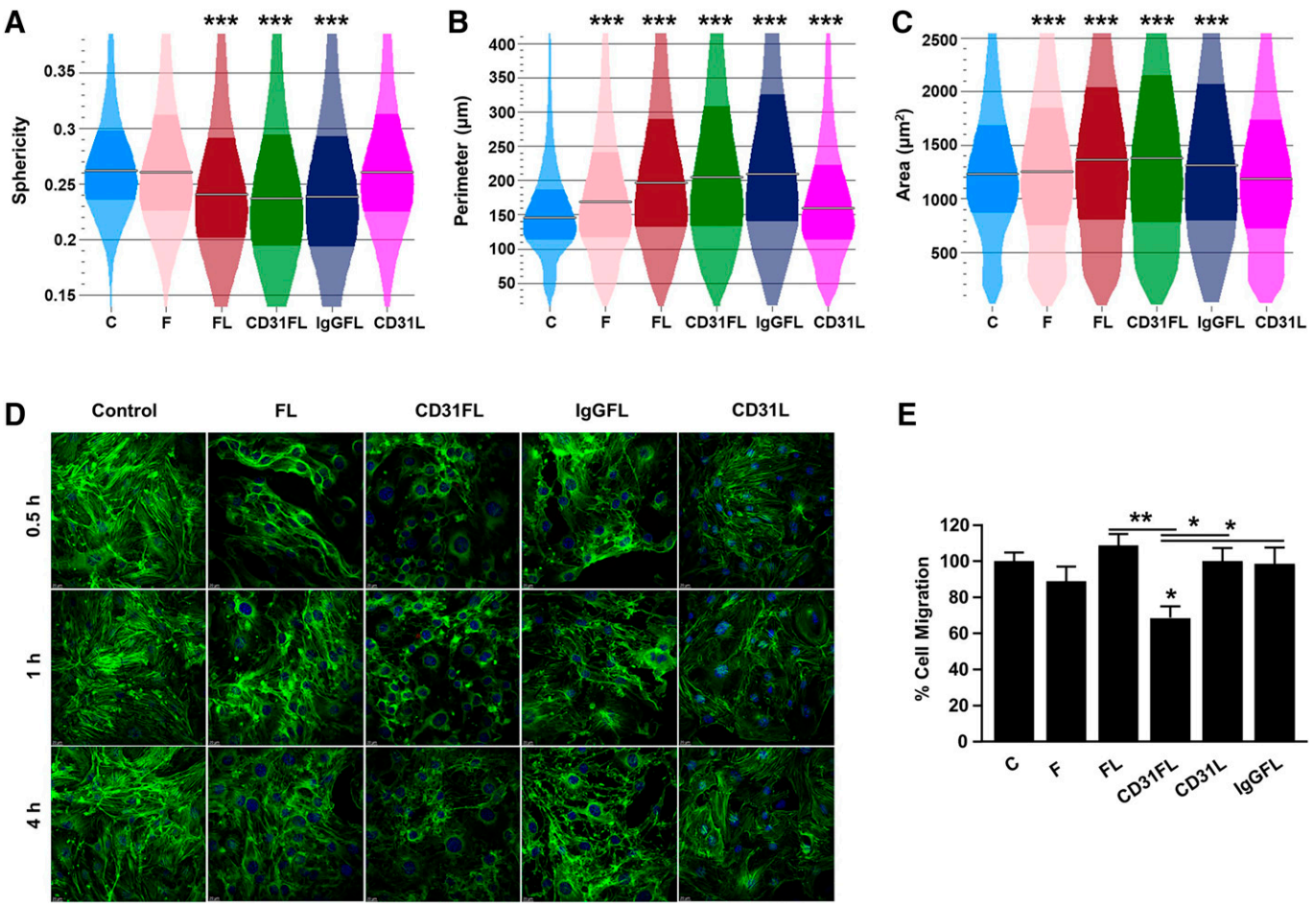

Fig. 8. Impact of liposomal nanoparticle treatment on morphometric parameters and stress fiber formation in b.End3 cells. (A–C) Calculation of cellular (A) sphericity, (B) perimeter, and (C) area of b.End3 cells upon incubation with F, FL, CD31FL, IgGFL, and CD31L (each group compared with the control) ($n > 24{,}500$ cells). (D) Representative immunofluorescence images demonstrating the impact of nanoparticle liposomes on stress fiber formation of b.End3 cells. (E) Quantification of basal migratory activity of b.End3 cells upon incubation with Fasudil or the aforementioned liposomal formulations (each group compared with the control) ($n = 3$). *$P < 0.05$; **$P < 0.01$; ***$P < 0.001$. C, control; CD31FL, CD31-targeting Fasudil liposomes; CD31L, CD31-targeting empty liposomes; F, Fasudil; FL, Fasudil liposomes; IgGFL, IgG-conjugated Fasudil liposomes.

2007; Chen et al., 2014). To assess whether encapsulated Fasudil in CD31 immunoliposomes presents optimal inhibitory effect of in vitro angiogenic functions, the effect of the CD31FL and control liposomes on angiogenesis, in terms of cell migration and tube formation on b.End3 cells, was explored.

Cell Migration. Treatment with CD31FL inhibited cell migration in a statistically significant manner compared with control, FL, and CD31L, demonstrating that the inhibition of endogenous b.End3 cell migration is due to the encapsulated Fasudil and the increased binding and, thus, uptake of the liposomes, whereas the CD31 antibody does not impact cell migration per se (Fig. 8E). Similar to FL, Fasudil and IgGFL did not significantly inhibit basal b.End3 cell migration (Fig. 8E), which shows that, contrary to the effect on morphometric parameters, cell migration inhibition is advantageous with the Fasudil in the CD31-targeting liposomes.

Tube Formation. To establish the optimal conditions for in vitro tube formation experiments of the b.End3 cells, 50,000 and 70,000 cells/well were resuspended in either starvation medium (control group) or complete medium (stimulated group) on a 2-dimensional Matrigel assay. When in higher confluency (70,000 cells/well), the b.End3 cells presented higher potency to form tubes, especially in complete medium conditions (Supplemental Fig. 2), as assessed by the number of nodes (Supplemental Fig. 2, A and D), number of junctions (Supplemental Fig. 2, B and D), and total sprout length (Supplemental Fig. 2, C and D). Therefore, the 70,000 cells/well for b.End3 cells was selected as the optimal cell number for the tube formation experiments with b.End3 cells, with the starvation conditions as the control/unstimulated groups and complete medium conditions as the stimulated groups. To assess the effect of the Fasudil-encapsulated liposomes on tube formation, the tube formation experiments were performed upon treatment with the different liposomal nanoparticles and nonencapsulated Fasudil. Treatment with complete media induced tube formation. Fasudil treatment partially inhibited the tube formation efficiency without significantly affecting the basal tube formation levels (starvation conditions; Fig. 9). A similar trend was exhibited with the remaining Fasudil-containing liposomal formulations (FL, IgGFL; Fig. 9). The Fasudil-lacking liposomal formulation (CD31L) also presented a partial, but significant, inhibition in the parameters assessed without affecting the basal tube formation levels, demonstrating some inhibitory trend from the liposomal formulation per se. This could signify that the energy consumed for liposomal endocytosis could partially impact other cellular

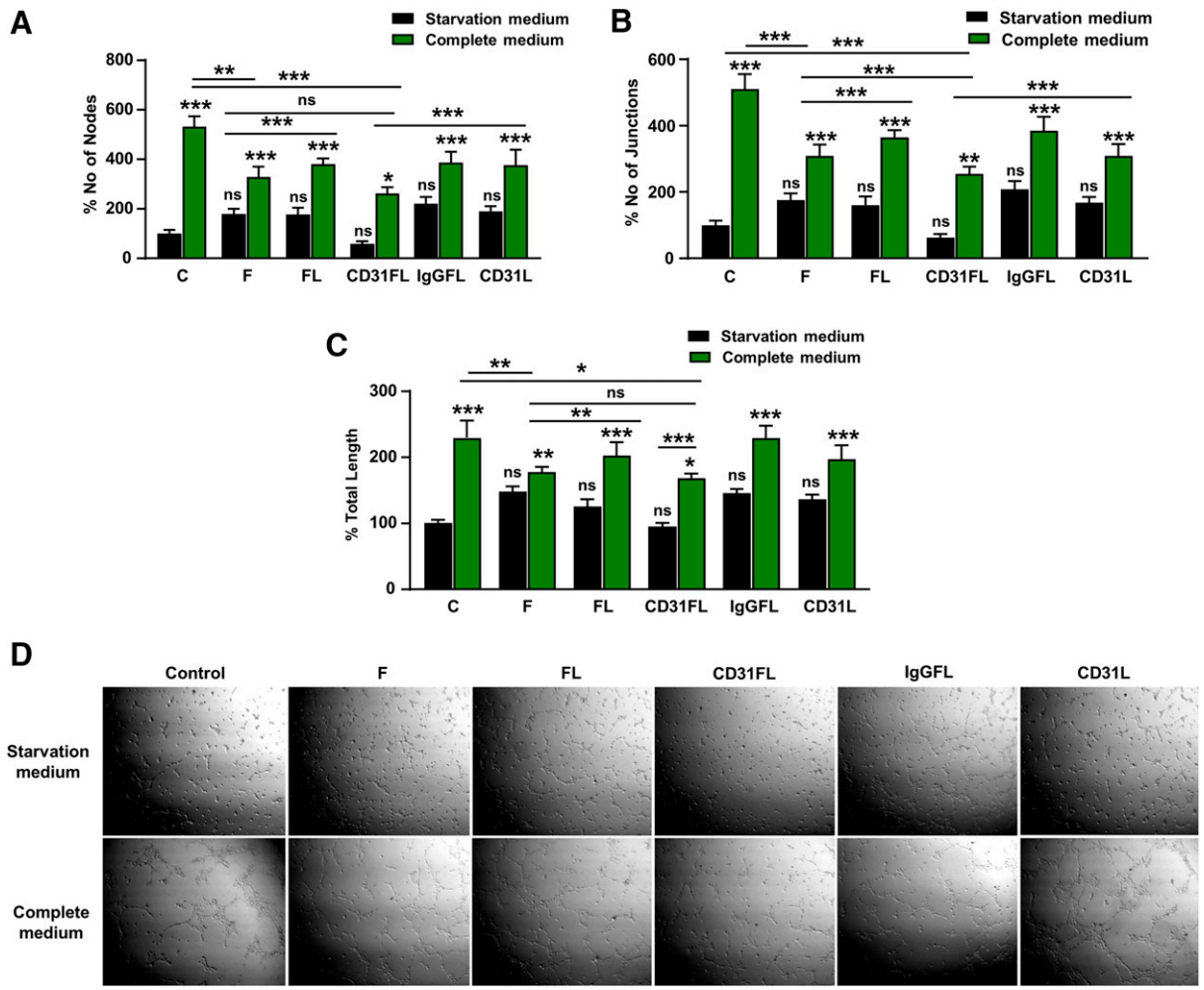

Fig. 9. Evaluation of the impact of liposomes on b.End3 cells' tube formation. (A–C) Quantification of (A) number of nodes, (B) number of junctions, and (C) total tubular length of b.End3-generated sprouts upon treatment with F, FL, CD31FL, IgGFL, and CD31L in starvation or complete medium (absence of lines, comparison with the control starvation group; lines indicate compared groups) ($n = 3$). (D) Representative images of the sprouts in each group. $^{*}P < 0.05$; $^{**}P < 0.01$; $^{***}P < 0.001$. C, control; CD31FL, CD31-targeting Fasudil liposomes; CD31L, CD31-targeting empty liposomes; F, Fasudil; FL, Fasudil liposomes; IgGFL, IgG-conjugated Fasudil liposomes; ns, not significant.

functions, including sprout formation. However, the cells treated with CD31FL exhibited decreased tube formation potential as shown by the different parameters: number of nodes (Fig. 9, A and D), number of junctions (Fig. 9, B and D), and total length (Fig. 9, C and D). Overall, tube formation was significantly decreased in most groups, compared with the control (Fig. 9, A–D), although the CD31FL group demonstrated the strongest, and statistically significant, inhibition from the CD31L group. As we compared nontargeted liposomes (FL), specific-targeted immunoliposomes with Fasudil (CD31FL), nonspecific-targeted immunoliposomes with Fasudil (IgGFL), and blank specific-targeted immunoliposomes (CD31L), our analysis precluded the potential for a CD31 antibody–mediated effect. Nonetheless, to exclude any confounding effects due to the presence of the antibodies on the liposomes, the tube formation experiments were performed at different concentrations of the IgG or CD31 antibodies alone (Supplemental Fig. 3). In comparison with the control group, no significant effects were observed on tube formation in all concentrations used for both antibodies, IgG (Supplemental Fig. 3, A–D), or CD31 (Supplemental Fig. 3, E–H). This rules out any confounding effects on angiogenesis that could be attributed to the CD31 antibody itself. Together, these findings show that CD31 antibody conjugation of the Fasudil liposomes offers a more robust inhibitory effect on tube formation and in vitro angiogenesis.

Discussion

The need for selective targeting and controlled drug release prompts wide utilization of nanotechnology for the development of new therapeutic options, and antibodies and antibody fragments are gaining popularity as targeting ligands (Marques et al., 2020). Inhibition of angiogenesis remains the main goal for several vascular-related diseases, including cancer, with tumor vessel normalization being the current goal for antiangiogenic therapy (Mattheolabakis and Mikelis, 2019). Despite the positive outcome of the current VEGF-targeting, antiangiogenic approaches, the resistance driven by the upregulation of other growth factors upon VEGF inhibition remains an important limitation (Wong et al., 2016; Mattheolabakis and Mikelis, 2019). We and others have previously highlighted the role of the small GTPase RhoA signaling in endothelial functions (Zeng et al., 2002; van Nieuw Amerongen et al., 2003; Zahra et al., 2019). In this study, we targeted the RhoA signaling in endothelial cells by

encapsulating the clinical-related ROCK inhibitor Fasudil in liposomes using the thin-film hydration method and evaluated the potential of this treatment approach using standard criteria (Mattheolabakis et al., 2012a; Gholizadeh et al., 2018a).

Several methods for antibody conjugation on nanoparticle surfaces have been developed over time (Gao et al., 2013; Oliveira et al., 2019; Juan et al., 2020). To ensure antigen binding and formation of the stable antibody-conjugated nanoparticles, we used maleimide chemistry, a frequent approach for covalent coupling of liposomes with an antibody's sulfhydryl group. A conjugation product, formed by the reaction between the antibody and the DSPE-PEG-maleimide, was attached to the surface of preformed liposomes at the postinsertion stage (Deng et al., 2013). Thiolation of antibodies was performed in the presence of Traut's reagent, a commonly used thiolating agent for this purpose. Removal of the excess of sulfhydryl-addition reagent was followed by the formation of the final conjugate between maleimide-modified nanoparticles and thiol-containing antibodies (Baiu et al., 2015).

TEM has previously been used to investigate bilayer organization, lamellar morphology, and the detection of flaws in bilayers (Zasadzinski, 1986; Gupta et al., 2013). Using TEM, no appreciable morphologic or structural changes were detected due to the antibody conjugation on the surface of the liposomes. Rather, we noticed a uniform bed of discrete spherical vesicles, which is in agreement with the size data obtained using the dynamic light scattering analysis.

The formulations were stored at 4°C for nearly 5 weeks with no significant changes in particle size and PDI, indicating that the vesicles did not form aggregates during the storage period. This can be attributed to the ζ potential value detected and steric stabilization provided by the PEG corona (Dos Santos et al., 2007), which prevented the particles from coalescing and aggregating. Furthermore, the lipids, cholesterol, and phospholipids used to prepare liposomes are unlikely to degrade during 4°C storage. These results corroborate with findings from other researchers (Haran et al., 1993).

Fasudil has a very low entrapment efficiency in lipid-based formulations because of its weakly basic hydrophilic nature (pKa = 9.727) (Gupta et al., 2013). This explains the encapsulation efficiency we observed. However, it's reported by other researchers that by switching to the active loading using $(NH_4)_2SO_4$-based transmembrane gradient method by varying pH of the rehydrating medium, the entrapment efficiency was enhanced by 2.5-fold (Gupta et al., 2013). Though our particles showed low encapsulation, the drug content was sufficient for use as a proof-of-concept study in targeted nanodelivery. An optimization of the encapsulation efficiency will be a significant focus of a future study.

The blood-brain barrier is a considerable obstacle for drug delivery (Lee and Leong, 2020). In our effort to target endothelial beds of different organs, we selected a general endothelial target that is also expressed in the blood-brain barrier endothelium. As such, we identified significant CD31 expression in the b.End3 cells, representing the murine blood-brain barrier endothelium. CD31 conjugation of the Fasudil-containing liposomes increased their binding by the b.End3 cells, which we hypothesized will greatly improve the delivery efficiency. It is important to note, however, that since the b.End3 is an endothelial-like cell line and not a primary endothelial cell, the angiogenic functions reported cannot exclusively represent endothelial cell functions.

The IC_{50} of Fasudil liposomes and antibody-conjugated Fasudil liposomes is slightly higher than that of free Fasudil. The increased IC_{50} values (lower cytotoxicity) of liposomal Fasudil may be due to steric hindrance from the PEG molecules on the liposomes' surface, which may delay Fasudil release or liposome uptake by the cells, when the liposomes come into contact with the cells (Mattheolabakis et al., 2012a) or due to Fasudil's antiapoptotic effects (Shi and Wei, 2007).

RhoA signaling regulates actin cytoskeletal changes, and our morphometric analysis via phase contrast–based live cell imaging exhibited a RhoA inhibition phenotype, as confirmed by the decrease in sphericity, which coincides with the increase in individual cell surface area and perimeter. In terms of morphometric parameters, these findings show that Fasudil-containing liposomes inhibit endothelial (b.End3) RhoA signaling. The ROCK/pMLC pathway is involved in actin cytoskeleton rearrangement (Matsui et al., 1996; Mikelis et al., 2015). The phalloidin staining (actin filamentation) demonstrates that compared with the other particles or free drug, CD31-congugated liposomal Fasudil encapsulation augmented the inhibition efficiency of stress fiber formation in endothelial cells.

Fasudil, a ROCK inhibitor, inhibits both angiogenesis and tumor-induced angiogenesis (Yin et al., 2007; Chen et al., 2014). FBS was selected as the positive control in our study due to the limited impact of VEGF on the tube formation of b.End3 cells (not shown). The lack of a statistically significant difference between the free antibody or antibody-conjugated empty liposomes compared with the control group rules out any confounding effect of antibody due to its interaction with the CD31 on the b.End3 cells. CD31 has been shown not to interact with VEGFR2 (Hwang et al., 2019), and although CD31 plays a role on angiogenesis (DeLisser et al., 1997), excess of our antibody did not, highlighting the importance of selecting proper antibodies for antibody-based nanoparticle targeting.

Overall, these findings demonstrate the feasibility of using CD31-targeting Fasudil liposomes as a potential targeted nanodelivery system in antiangiogenic therapy and further highlight the potential of the RhoA signaling pathway as a significant target for angiogenesis inhibition. Further evaluation, including in vivo studies, is required to define their anticancer potential.

Acknowledgments

The authors thank the members of Mikelis laboratory for their critical review of the manuscript. Figure 1 was created with Biorender.com.

Authorship Contributions

Participated in research design: Lahooti, Mattheolabakis, Mikelis.

Conducted experiments: Lahooti, Akwii, Patel, ShahbaziNia, Lamprou.

Contributed new reagents and analytic tools: Abbruscato, Astrinidis, Bickel, Al-Ahmad, German.

Performed data analysis: Lahooti, Madadi, Mattheolabakis, Mikelis.

Wrote or contributed to the writing of the manuscript: Lahooti, Bickel, German, Mattheolabakis, Mikelis.

References

Akhtar MJ, Ahamed M, Alhadlaq HA, Alrokayan SA, and Kumar S (2014) Targeted anticancer therapy: overexpressed receptors and nanotechnology. *Clin Chim Acta* **436**:78–92.

Akwii RG, Sajib MS, Zahra FT, Tullar P, Zabet-Moghaddam M, Zheng Y, Silvio Gutkind J, Doci CL, and Mikelis CM (2022) Angiopoietin-2-induced lymphatic endothelial cell

migration drives lymphangiogenesis via the β1 integrin-RhoA-formin axis. *Angiogenesis* **25**:373–396.
Attia MF, Anton N, Wallyn J, Omran Z, and Vandamme TF (2019) An overview of active and passive targeting strategies to improve the nanocarriers efficiency to tumour sites. *J Pharm Pharmacol* **71**:1185–1198.
Baiu DC, Artz NS, McElreath MR, Menapace BD, Hernando D, Reeder SB, Grüttner C, and Otto M (2015) High specificity targeting and detection of human neuroblastoma using multifunctional anti-GD2 iron-oxide nanoparticles. *Nanomedicine (Lond)* **10**:2973–2988.
Barry DM, Xu K, Meadows SM, Zheng Y, Norden PR, Davis GE, and Cleaver O (2015) Cdc42 is required for cytoskeletal support of endothelial cell adhesion during blood vessel formation in mice. *Development* **142**:3058–3070.
Barua S and Mitragotri S (2014) Challenges associated with Penetration of Nanoparticles across Cell and Tissue Barriers: A Review of Current Status and Future Prospects. *Nano Today* **9**:223–243.
Bazak R, Houri M, El Achy S, Kamel S, and Refaat T (2015) Cancer active targeting by nanoparticles: a comprehensive review of literature. *J Cancer Res Clin Oncol* **141**:769–784.
Botosoa EP, Maillasson M, Mougin-Degraef M, Remaud-Le Saëc P, Gestin JF, Jacques Y, Barbet J, and Faivre-Chauvet A (2011) Antibody-Hapten Recognition at the Surface of Functionalized Liposomes Studied by SPR: Steric Hindrance of Pegylated Phospholipids in Stealth Liposomes Prepared for Targeted Radionuclide Delivery. *J Drug Deliv* **2011**:368535.
Bryan BA, Dennstedt E, Mitchell DC, Walshe TE, Noma K, Loureiro R, Saint-Geniez M, Campaigniac JP, Liao JK, and D'Amore PA (2010) RhoA/ROCK signaling is essential for multiple aspects of VEGF-mediated angiogenesis. *FASEB J* **24**:3186–3195.
Bulbake U, Doppalapudi S, Kommineni N, and Khan W (2017) Liposomal Formulations in Clinical Use: An Updated Review. *Pharmaceutics* **9**:12.
Chen W, Mao K, Hua-Huy T, Bei Y, Liu Z, and Dinh-Xuan AT (2014) Fasudil inhibits prostate cancer-induced angiogenesis in vitro. *Oncol Rep* **32**:2795–2802.
DeLisser HM, Christofidou-Solomidou M, Strieter RM, Burdick MD, Robinson CS, Wexler RS, Kerr JS, Garlanda C, Merwin JR, Madri JA, et al. (1997) Involvement of endothelial PECAM-1/CD31 in angiogenesis. *Am J Pathol* **151**:671–677.
Deng L, Zhang Y, Ma L, Jing X, Ke X, Lian J, Zhao Q, Yan B, Zhang J, Yao J, et al. (2013) Comparison of anti-EGFR-Fab' conjugated immunoliposomes modified with two different conjugation linkers for siRNa delivery in SMMC-7721 cells. *Int J Nanomedicine* **8**:3271–3283.
Dos Santos N, Allen C, Doppen AM, Anantha M, Cox KA, Gallagher RC, Karlsson G, Edwards K, Kenner G, Samuels L, et al. (2007) Influence of poly(ethylene glycol) grafting density and polymer length on liposomes: relating plasma circulation lifetimes to protein binding. *Biochim Biophys Acta* **1768**:1367–1377.
Fava A, Wung PK, Wigley FM, Hummers LK, Daya NR, Ghazarian SR, and Boin F (2012) Efficacy of Rho kinase inhibitor fasudil in secondary Raynaud's phenomenon. *Arthritis Care Res (Hoboken)* **64**:925–929.
Gao J, Chen H, Song H, Su X, Niu F, Li W, Li B, Dai J, Wang H, and Guo Y (2013) Antibody-targeted immunoliposomes for cancer treatment. *Mini Rev Med Chem* **13**:2026–2035.
Garnacho C, Shuvaev V, Thomas A, McKenna L, Sun J, Koval M, Albelda S, Muzykantov V, and Muro S (2008) RhoA activation and actin reorganization involved in endothelial CAM-mediated endocytosis of anti-PECAM carriers: critical role for tyrosine 686 in the cytoplasmic tail of PECAM-1. *Blood* **111**:3024–3033.
Gholizadeh S, Dolman EM, Wieriks R, Sparidans RW, Hennink WE, and Kok RJ (2018a) Anti-GD2 Immunoliposomes for Targeted Delivery of the Survivin Inhibitor Sepantronium Bromide (YM155) to Neuroblastoma Tumor Cells. *Pharm Res* **35**:85.
Gholizadeh S, Visweswaran GRR, Storm G, Hennink WE, Kamps JAAM, and Kok RJ (2018b) E-selectin targeted immunoliposomes for rapamycin delivery to activated endothelial cells. *Int J Pharm* **548**:759–770.
Girão-Silva T, Fonseca-Alaniz MH, Ribeiro-Silva JC, Lee J, Patil NP, Dallan LA, Baker AB, Harmsen MC, Krieger JE, and Miyakawa AA (2021) High stretch induces endothelial dysfunction accompanied by oxidative stress and actin remodeling in human saphenous vein endothelial cells. *Sci Rep* **11**:13493.
Girshovitz P and Shaked NT (2012) Generalized cell morphological parameters based on interferometric phase microscopy and their application to cell life cycle characterization. *Biomed Opt Express* **3**:1757–1773.
Gupta V, Gupta N, Shaik IH, Mehvar R, McMurtry IF, Oka M, Nozik-Grayck E, Komatsu M, and Ahsan F (2013) Liposomal fasudil, a rho-kinase inhibitor, for prolonged pulmonary preferential vasodilation in pulmonary arterial hypertension. *J Control Release* **167**:189–199.
Han J, Shuvaev VV, Davies PF, Eckmann DM, Muro S, and Muzykantov VR (2015) Flow shear stress differentially regulates endothelial uptake of nanocarriers targeted to distinct epitopes of PECAM-1. *J Control Release* **210**:39–47.
Han J, Zern BJ, Shuvaev VV, Davies PF, Muro S, and Muzykantov V (2012) Acute and chronic shear stress differently regulate endothelial internalization of nanocarriers targeted to platelet-endothelial cell adhesion molecule-1. *ACS Nano* **6**:8824–8836.
Haran G, Cohen R, Bar LK, and Barenholz Y (1993) Transmembrane ammonium sulfate gradients in liposomes produce efficient and stable entrapment of amphipathic weak bases. *Biochim Biophys Acta* **1151**:201–215.
Hermanson GT, editor (2013) Chapter 3 - The reactions of Bioconjugation, in *Bioconjugate Techniques*, 3rd ed, pp 229–258, Elsevier, Netherlands.
Hwang MS, Strainic MG, Pohlmann E, Kim H, Pluskota E, Ramirez-Bergeron DL, Plow EF, and Medof ME (2019) VEGFR2 survival and mitotic signaling depends on joint activation of associated C3ar1/C5ar1 and IL-6R-gp130. *J Cell Sci* **132**:jcs219352.
Juan A, Cimas FJ, Bravo I, Pandiella A, Ocaña A, and Alonso-Moreno C (2020) Antibody Conjugation of Nanoparticles as Therapeutics for Breast Cancer Treatment. *Int J Mol Sci* **21**:6018.
Laviña B, Castro M, Niaudet C, Cruys B, Álvarez-Aznar A, Carmeliet P, Bentley K, Brakebusch C, Betsholtz C, and Gaengel K (2018) Defective endothelial cell migration in the absence of Cdc42 leads to capillary-venous malformations. *Development* **145**:dev161182.
Lee CS and Leong KW (2020) Advances in microphysiological blood-brain barrier (BBB) models towards drug delivery. *Curr Opin Biotechnol* **66**:78–87.
Li H, Wang X, Guo X, Wan Q, Teng Y, and Liu J (2022) Development of rapamycin-encapsulated exosome-mimetic nanoparticles-in-PLGA microspheres for treatment of hemangiomas. *Biomed Pharmacother* **148**:112737.
Lu L, Ding Y, Zhang Y, Ho RJ, Zhao Y, Zhang T, and Guo C (2018) Antibody-modified liposomes for tumor-targeting delivery of timosaponin AIII. *Int J Nanomedicine* **13**:1927–1944.
Lyu Y, Xiao Q, Yin L, Yang L, and He W (2019) Potent delivery of an MMP inhibitor to the tumor microenvironment with thermosensitive liposomes for the suppression of metastasis and angiogenesis. *Signal Transduct Target Ther* **4**:26.
Marques AC, Costa PJ, Velho S, and Amaral MH (2020) Functionalizing nanoparticles with cancer-targeting antibodies: A comparison of strategies. *J Control Release* **320**:180–200.
Matsui T, Amano M, Yamamoto T, Chihara K, Nakafuku M, Ito M, Nakano T, Okawa K, Iwamatsu A, and Kaibuchi K (1996) Rho-associated kinase, a novel serine/threonine kinase, as a putative target for small GTP binding protein Rho. *EMBO J* **15**:2208–2216.
Mattheolabakis G and Mikelis CM (2019) Nanoparticle Delivery and Tumor Vascular Normalization: The Chicken or The Egg? *Front Oncol* **9**:1227.
Mattheolabakis G, Nie T, Constantinides PP, and Rigas B (2012a) Sterically stabilized liposomes incorporating the novel anticancer agent phospho-ibuprofen (MDC-917): preparation, characterization, and in vitro/in vivo evaluation. *Pharm Res* **29**:1435–1443.
Mattheolabakis G, Rigas B, and Constantinides PP (2012b) Nanodelivery strategies in cancer chemotherapy: biological rationale and pharmaceutical perspectives. *Nanomedicine (Lond)* **7**:1577–1590.
Mikelis C, Lamprou M, Koutsioumpa M, Koutsioubas AG, Spyranti Z, Zompra AA, Spiliopoulos N, Vradis AA, Katsoris P, Spyroulias GA, et al. (2011) A peptide corresponding to the C-terminal region of pleiotrophin inhibits angiogenesis in vivo and in vitro. *J Cell Biochem* **112**:1532–1543.
Mikelis CM, Palmby TR, Simaan M, Li W, Szabo R, Lyons R, Martin D, Yagi H, Fukuhara S, Chikumi H, et al. (2013) PDZ-RhoGEF and LARG are essential for embryonic development and provide a link between thrombin and LPA receptors and Rho activation. *J Biol Chem* **288**:12232–12243.
Mikelis CM, Simaan M, Ando K, Fukuhara S, Sakurai A, Amornphimoltham P, Masedunskas A, Weigert R, Chavakis T, Adams RH, et al. (2015) RhoA and ROCK mediate histamine-induced vascular leakage and anaphylactic shock. *Nat Commun* **6**:6725.
Murciano JC, Harshaw DW, Ghitescu L, Danilov SM, and Muzykantov VR (2001) Vascular immunotargeting to endothelial surface in a specific macrodomain in alveolar capillaries. *Am J Respir Crit Care Med* **164**:1295–1302.
Nohata N, Uchida Y, Stratman AN, Adams RH, Zheng Y, Weinstein BM, Mukouyama YS, and Gutkind JS (2016) Temporal-specific roles of Rac1 during vascular development and retinal angiogenesis. *Dev Biol* **411**:183–194.
Nohria A, Grunert ME, Rikitake Y, Noma K, Prsic A, Ganz P, Liao JK, and Creager MA (2006) Rho kinase inhibition improves endothelial function in human subjects with coronary artery disease. *Circ Res* **99**:1426–1432.
Oliveira JP, Prado AR, Keijok WJ, Antunes PWP, Yapuchura ER, and Guimarães MCC (2019) Impact of conjugation strategies for targeting of antibodies in gold nanoparticles for ultrasensitive detection of 17β-estradiol. *Sci Rep* **9**:13859.
Parhiz H, Shuvaev VV, Pardi N, Khoshnejad M, Kiseleva RY, Brenner JS, Uhler T, Tuyishime S, Mui BL, Tam YK, et al. (2018) PECAM-1 directed re-targeting of exogenous mRNA providing two orders of magnitude enhancement of vascular delivery and expression in lungs independent of apolipoprotein E-mediated uptake. *J Control Release* **291**:106–115.
Pattni BS, Chupin VV, and Torchilin VP (2015) New Developments in Liposomal Drug Delivery. *Chem Rev* **115**:10938–10966.
Pepper MS (1997) Manipulating angiogenesis. From basic science to the bedside. *Arterioscler Thromb Vasc Biol* **17**:605–619.
Prasad S, Sajja RK, Kaisar MA, Park JH, Villalba H, Liles T, Abbruscato T, and Cucullo L (2017) Role of Nrf2 and protective effects of Metformin against tobacco smoke-induced cerebrovascular toxicity. *Redox Biol* **12**:58–69.
Ravasco JMJM, Faustino H, Trindade A, and Gois PMP (2019) Bioconjugation with Maleimides: A Useful Tool for Chemical Biology. *Chemistry* **25**:43–59.
Ridley AJ (2015) Rho GTPase signalling in cell migration. *Curr Opin Cell Biol* **36**:103–112.
Ringgaard L, Melander F, Eliasen R, Henriksen JR, Jølck RI, Engel TB, Bak M, Fliedner FP, Kristensen K, Elema DR, et al. (2020) Tumor repolarization by an advanced liposomal drug delivery system provides a potent new approach for chemoimmunotherapy. *Sci Adv* **6**:eaba5628.
Shi J and Wei L (2007) Rho kinase in the regulation of cell death and survival. *Arch Immunol Ther Exp (Warsz)* **55**:61–75.
Sigurdardottir AK, Jonasdottir AS, Asbjarnarson A, Helgudottir HR, Gudjonsson T, and Traustadottir GA (2021) Peroxidasin Enhances Basal Phenotype and Inhibits Branching Morphogenesis in Breast Epithelial Progenitor Cell Line D492. *J Mammary Gland Biol Neoplasia* **26**:321–338.
Sun S, Zou H, Li L, Liu Q, Ding N, Zeng L, Li H, and Mao S (2019) CD123/CD33 dual-antibody modified liposomes effectively target acute myeloid leukemia cells and reduce antigen-negative escape. *Int J Pharm* **568**:118518.
Tan W, Palmby TR, Gavard J, Amornphimoltham P, Zheng Y, and Gutkind JS (2008) An essential role for Rac1 in endothelial cell function and vascular development. *FASEB J* **22**:1829–1838.
Twentyman PR and Luscombe M (1987) A study of some variables in a tetrazolium dye (MTT) based assay for cell growth and chemosensitivity. *Br J Cancer* **56**:279–285.
van Nieuw Amerongen GP, Koolwijk P, Versteilen A, and van Hinsbergh VW (2003) Involvement of RhoA/Rho kinase signaling in VEGF-induced endothelial cell migration and angiogenesis in vitro. *Arterioscler Thromb Vasc Biol* **23**:211–217.
Wang F, Li Y, Jiang H, Li C, Li Z, Qi C, Li Z, Gao Z, Zhang B, and Wu J (2021) Dual-Ligand-Modified Liposomes Co-Loaded with Anti-Angiogenic and Chemotherapeutic Drugs for Inhibiting Tumor Angiogenesis and Metastasis. *Int J Nanomedicine* **16**:4001–4016.

Whittenton J, Pitchumani R, Thevananther S, and Mohanty K (2013) Evaluation of asymmetric immunoliposomal nanoparticles for cellular uptake. *J Microencapsul* **30**:55–63.
Wong PP, Bodrug N, and Hodivala-Dilke KM (2016) Exploring Novel Methods for Modulating Tumor Blood Vessels in Cancer Treatment. *Curr Biol* **26**:R1161–R1166.
Yang W, Hu Q, Xu Y, Liu H, and Zhong L (2018) Antibody fragment-conjugated gemcitabine and paclitaxel-based liposome for effective therapeutic efficacy in pancreatic cancer. *Mater Sci Eng C* **89**:328–335.
Yin L, Morishige K, Takahashi T, Hashimoto K, Ogata S, Tsutsumi S, Takata K, Ohta T, Kawagoe J, Takahashi K, et al. (2007) Fasudil inhibits vascular endothelial growth factor-induced angiogenesis in vitro and in vivo. *Mol Cancer Ther* **6**:1517–1525.
Zahra FT, Sajib MS, Ichiyama Y, Akwii RG, Tullar PE, Cobos C, Minchew SA, Doçi CL, Zheng Y, Kubota Y, et al. (2019) Endothelial RhoA GTPase is essential for in vitro endothelial functions but dispensable for physiological in vivo angiogenesis. *Sci Rep* **9**:11666.
Zahra FT, Sajib MS, and Mikelis CM (2021) Role of bFGF in Acquired Resistance upon Anti-VEGF Therapy in Cancer. *Cancers (Basel)* **13**:1422.
Zasadzinski JA (1986) Transmission electron microscopy observations of sonication-induced changes in liposome structure. *Biophys J* **49**:1119–1130.
Zeng H, Zhao D, and Mukhopadhyay D (2002) KDR stimulates endothelial cell migration through heterotrimeric G protein Gq/11-mediated activation of a small GTPase RhoA. *J Biol Chem* **277**:46791–46798.
Zhang C, Chen Z, Li W, Liu X, Tang S, Jiang L, Li M, Peng H, and Lian M (2020) Influences of different sugar ligands on targeted delivery of liposomes. *J Drug Target* **28**:789–801.

Address correspondence to: George Mattheolabakis, School of Basic Pharmaceutical and Toxicological Sciences, College of Pharmacy, University of Louisiana Monroe, Monroe, LA 71209. E-mail: matthaiolampakis@ulm.edu; or Constantinos M. Mikelis, Laboratory of Molecular Pharmacology, Department of Pharmacy, University of Patras, Patras 26504, Greece & Department of Pharmaceutical Sciences, School of Pharmacy, Texas Tech University Health Sciences Center, Amarillo, TX 79106. E-mail: kmikelis@upatras.gr